

# The Evolution of Dust Opacity in Galaxies.

Daniela Calzetti

Space Telescope Science Institute, 3700 San Martin Dr., Baltimore, MD 21218, USA; e-mail: calzetti@stsci.edu

and

Timothy M. Heckman<sup>1</sup>

Dept. of Physics and Astronomy, The Johns Hopkins University, Baltimore, MD 21218, USA; e-mail: heckman@pha.jhu.edu

## ABSTRACT

We investigate the evolution of the opacity of galaxies as a function of redshift, using simple assumptions about the metal and dust enrichment of the gas and the distribution of dust in galaxies. The method presented in this paper uses an iterative procedure to reconstruct the intrinsic Star Formation Rate (SFR) density of galaxies as a function of redshift, by correcting the observed UV emission for the obscuring effects of the dust produced by the star formation itself. Where necessary, gas inflows/outflows are included to dilute/remove the excess of metals produced by the stars for fixed yield. The iterative procedure converges to multiple solutions for the intrinsic SFR density, divided into two basic classes. The first class of solutions predicts a relatively large amount of UV attenuation at high redshift, with  $A_{1500\text{\AA}} = 1.9$  mag at  $z \sim 3$ , and smaller attenuations at low redshift ( $z < 1$ ), with  $A_{2800\text{\AA}} = 1.25$  mag. The SFR density of this set of solutions is constant for  $z \gtrsim 1.2$  and declines for  $z < 1.2$ ; it resembles in shape the “monolithic collapse” scenario for star formation. The second class of solutions predicts relatively low UV attenuations at high redshift, with  $A_{1500\text{\AA}} = 0.75$  mag at  $z \sim 3$ , and larger attenuations at low redshift, with  $A_{2800\text{\AA}} = 1.50$  mag at  $z < 1$ . The SFR density in this case has a peak at  $z \simeq 1.2$ . The advantages and shortcomings of both classes are analyzed in the light of available observational constraints, including the opacity of galaxies at  $0 \leq z \leq 1$  and the intensity and spectral energy distribution of the cosmic infrared background from the COBE DIRBE and FIRAS data. We conclude that both classes of models are acceptable within the current uncertainties, but the “monolithic collapse” class matches the available observations better than the other one. We also investigate the dependence of our solutions on the different model assumptions.

*Subject headings:* Galaxies: Evolution – Galaxies: ISM – ISM: Dust, Extinction

---

<sup>1</sup>Adjunct Astronomer at the Space Telescope Science Institute.

## 1. Introduction

One of the fundamental elements of the study of the evolution of the Universe is the investigation of how the light evolves. The bulk of the observed light is given by the stellar component of galaxies, and measuring the light and its spectral energy distribution measures the total stellar content and the star formation history of galaxies. Using ultraviolet (UV) data from the Canada-France Redshift Survey (Lilly et al. 1996) and from the HDF (Williams et al. 1996), Madau et al. (1996) estimated the cosmic star formation rate density of galaxies. The UV emission is more directly related to the star formation rate (SFR) than emission at longer wavelengths, because most of the UV light below  $3,000 \text{ \AA}$  is emitted by hot, massive, relatively short-lived ( $<1 \text{ Gyr}$ ) stars. In addition, the rest frame UV is the most readily accessible wavelength range in high redshift galaxies with standard (optical) observing techniques.

One of the problems which haunts the UV determinations of the cosmic SFR density is the potentially large uncertainty introduced by dust obscuration. Star formation comes together with metal production and, therefore, dust. The timescales for the formation of dust are short,  $\sim 100\text{-}200 \text{ Myr}$  (Tielens 1990, Jones et al. 1994, Dwek 1998), and dust opacity may affect the emerging light fairly early in the history of a galaxy. Dust extinction is more effective at shorter wavelengths, so the rest frame UV light is more affected than the optical or IR emission. The degree to which the light is affected is, however, difficult to quantify as the metal (and dust) content per unit mass is only one of the parameters to take into account; for instance, the opacity of a galaxy is also determined by its gas fraction. Although present-day galaxies are more metal rich than high redshift galaxies, they could be less opaque; they have locked a large fraction of their gas into stars, thus removing dust from the interstellar medium. In the past, more gas was available per unit mass; thus even small metallicities had potentially large effects in terms of the obscuring power of the associated dust. Last, but not least, is the uncertainty introduced by the unknown distribution of the dust in the galaxy. The effects on the emerging UV-optical light of various geometries of emitters and absorbers have been discussed by a number of authors (to name a few, Rowan-Robinson & Crawford 1989, Witt, Thronson & Capuano 1992, Calzetti, Kinney & Storchi-Bergmann 1994, Witt & Gordon 1996), and this is the largest uncertainty in any model of galaxy opacity.

The problem of dust obscuration in the derivation of the cosmic SFR density is widely recognized and different authors have taken different approaches to it. Pei & Fall (1995) introduce dust in their treatment of the evolution of Damped Lyman- $\alpha$  systems (DLAs) to account for missing high metallicity systems in high redshift surveys. Meurer et al. (1997) have been among the first to raise the issue for Lyman-break galaxies, by noticing that the UV spectral energy distributions of these objects (Steidel et al. 1996) are too red to be dust-free star-forming galaxies. They attempt a correction for dust reddening of the high redshift galaxies by extrapolating a method used for local starburst galaxies (Calzetti et al. 1994). Sawicki & Yee (1998) reach similar conclusions using a wider photometric baseline. Rowan-Robinson et al. (1997) use ISO observations to derive the star formation rate at high redshift from the far-infrared emission of

galaxies. Renzini (1997) uses evidence on the metal enrichment of the intracluster medium (see, e.g., Yamashita 1992) to infer the amount of high redshift star formation required to produce the observed mass in metals. Mushotzky & Loewenstein (1997) use the lack of evolution in the metal abundance of galaxy clusters to conclude that most of the metal enrichment occurred at  $z > 1$  and, thus, star formation had to be higher than measured from UV-optical surveys. Madau, Pozzetti, & Dickinson (1998) discuss the case of a simple model of foreground dust with increasing opacity as a function of redshift, imposing negligible dust correction at low redshift and a factor  $\sim 5$  in the UV flux at  $z \sim 3$ . In all cases, there is no attempt to obtain a self-consistent solution between the correction factor imposed to the global SFR density (derived from the UV light of galaxies) and the UV opacity such SFR density implies.

There is mounting evidence that galaxies in the local Universe are generally not very opaque, although the quantification of this statement is still under debate. With techniques which use illuminating background sources (e.g.: White, Keel & Conselice 1996, Berlind et al. 1997, Gonzalez et al. 1998), spiral galaxies are shown to have transparent interarm regions at optical wavelengths, with  $A_B \sim A_I \sim 0.1-0.2$ , and opaque arms, with  $A_B \sim A_I \sim 1$ . The same level of opacity as the arms is found in the centers of the spirals (Giovanelli et al. 1995, Moriondo, Giovanelli & Haynes 1998). As expected, the opaque regions of spirals coincide with the regions of most intense star formation (the arms), as stars form in the dusty molecular clouds. The UV-optical energy absorbed by dust is re-radiated in the FIR at wavelengths longer than a few  $\mu\text{m}$ . The energy balance between the UV-optical and the Far-Infrared (FIR) emission from disk galaxies reveals that the amount of stellar light absorbed by dust and re-emitted in the FIR range is about the same as the emerging stellar light (Soifer & Neugebauer 1991, Xu & Buat 1995, Wang & Heckman 1996, Trewhella 1997). Preliminary results from ISO observations of the CFRS galaxies indicate that about 55% of the star formation at  $z < 1$  emerges in the FIR (Hammer & Flores 1998). Local ( $z \leq 0.1$ ) surveys in  $\text{H}\alpha$  show that the SFR derived from the nebular emission line luminosity density is about a factor  $\sim 3$  higher than the low redshift extrapolation of the CFRS UV measurements (Gronwall 1998, see, however, Gallego et al. 1995), suggesting that the lower value of SFR from the UV may be due to dust obscuration. The low-redshift issue, however, is not settled: Treyer et al. (1998) find that their UV data from FOCA also produce a local ( $z \sim 0.15$ ) value of the SFR which is a factor  $\sim 2-3$  larger than the extrapolation from the CFRS UV data. Although none of the above results can be considered final, the available data suggest that dust absorbs a factor  $\sim 1/2$ , and probably no more than  $2/3$ , of the total stellar light in local galaxies.

The situation is even less clear at high redshift, as long wavelength baselines are available only for a handful of high redshift galaxies. The optical and near-IR rest frame of distant galaxies is in the near-mid IR range, and ground-based measurements are less sensitive at these wavelengths. On the basis of the UV slope alone, Meurer et al. (1997) suggest a factor 10 attenuation of the  $1500 \text{ \AA}$  flux of the Lyman-break galaxies at  $z \sim 3$ , although recent revisions bring the attenuation correction down to 5.5 (Meurer, Heckman & Calzetti 1998). The addition of near-IR data points brings the  $1500 \text{ \AA}$  attenuation at  $z \sim 3$  into the factor range 2.5–7 (Dickinson 1998). The ISO

FIR emission of high redshift galaxies in the Hubble Deep Field indicates a correction factor closer to  $\sim 5$  at  $z > 2$  (Rowan-Robinson et al. 1997). The nebular line emission of six of the Lyman-break galaxies from near-IR spectroscopy also suggest corrections between 3 and 6 for the flux at  $1500 \text{ \AA}$  (Pettini et al. 1998a). Optical/near-IR nebular line ratios and CO detections have provided additional observational evidence for dust at redshifts as high as  $z=4.70$  in several individual objects, usually radio galaxies (e.g., Dey, Spinrad & Dickinson 1995, Armus et al. 1998a) and AGNs (e.g., Omont et al. 1996, Ivison et al. 1998). Also, indirect evidence for presence of dust in a  $z=5.34$  galaxy has been presented by Armus et al. (1998b).

Current measurements of the cosmic infrared background (CIB) from COBE DIRBE (Hauser et al. 1998) and FIRAS (Fixsen et al. 1998) imply a non-negligible FIR emission from dust in galaxies. For instance, the DIRBE data give  $\nu I(\nu)=25\pm 7 \text{ nW m}^{-2} \text{ sr}^{-1}$  at  $140 \mu\text{m}$  and  $14\pm 3 \text{ nW m}^{-2} \text{ sr}^{-1}$  at  $240 \mu\text{m}$ , which imply a CIB emission between 2 and 3 times higher than the combined emission of the UV+optical+near-IR backgrounds (Madau et al. 1998). Still unknown is the mean redshift of the galaxies from which the bulk of the CIB arises. Recent observations obtained at  $450 \mu\text{m}$  and  $850 \mu\text{m}$  with SCUBA at the JCMT (Smail, Ivison & Blain 1997, Hughes et al. 1998, Barger et al. 1998, Eales et al. 1998) have attempted to address this issue by probing the FIR emission of individual high redshift galaxies. The SCUBA data should provide a measure of the intrinsic, reddening-free SFR in high redshift galaxies as much as the IRAS data provide a measure of the intrinsic SFR in local starburst galaxies (e.g., Young et al. 1989). The SCUBA detections are consistent with many of the objects being at  $z \geq 1$ ; the inferred SFRs have values  $\sim 2\text{--}5$  times higher than those derived from the restframe UV detections in the same redshift range. However, in the local Universe the brightest FIR emitters are generally AGNs or powerful starbursts, like Arp220, and the nature of the SCUBA galaxies (AGN/starburst) has not been settled yet. In addition difficulties in the redshift assignment leave some of the interpretation still open for debate. The flux density of the current SCUBA sources amounts to about 20–30% of the COBE background at  $850 \mu\text{m}$ , and the number density is only 1/10 of the optical high redshift galaxies (Lilly et al. 1998).

The aim of this paper is to model the average opacity of galaxies as a function of both redshift and wavelength. We mainly concentrate on the effects of dust on the ensemble of restframe UV photons produced by galaxies throughout cosmic times. The basic philosophy is the following. Star formation produces metals and, thus, dust. The global SFR density of galaxies is derived from the observed UV luminosities, which are sensitive to dust opacity. We solve self-consistently for the intrinsic global SFR density and for the effects of the dust created by the star formation itself, till we reproduce the observed UV flux density. Simple assumptions about the cosmology, and the galaxy and dust models allow us to budget the fraction of light lost to dust obscuration at each redshift. From the computed opacities, we then derive the intensity and the spectral energy distribution of the CIB, which we compare with the observational data from COBE DIRBE and FIRAS. Additional observational constraints, such as DLAs and SCUBA measurements at high redshift, and the energy density in the local Universe at FIR (both IRAS and ISO),  $H\alpha$ , and radio

wavelengths are used to further validate the solutions. Finally, we discuss the impact of our input assumptions on the results.

In the following, we adopt a cosmology with  $H_0=50$  km/s/Mpc and  $q_0=0.5$ .

## 2. The Model

For standard assumptions as to the cosmology, the metal and dust enrichment, and the distribution of dust in galaxies, we follow in time the evolution and appearance of the average galaxy from the beginning of the star formation to the present. Here galaxies are assumed to be already gravitationally bound, although not closed, systems. Only the evolution of the stellar, metal, and dust contents is implemented. Edmunds & Phillips (1997) present an extensive treatment of the chemical evolution of galaxies for different assumptions about the star formation history and galaxy model (closed-box/inflow/outflow). Their work is in the same vein as Pei & Fall (1995), who discuss the evolution of DLAs. The main difference between our and those authors' approach is that we do not adopt an *a priori* global SFR density; rather, we start from the observed one, derived from the UV flux density of galaxies, and correct it iteratively for the associated UV dust opacities, until the corrections match the predicted obscuration. The observed global SFR density predicts non-zero UV dust opacity from the simple act of forming stars. These opacities are fed back into the SFR density in the form of correction factors; the evolution of the star, metal and dust content of galaxies is followed again and new opacities derived. The iterative procedure is stopped when the corrections to the global SFR density differ  $1 \sigma$  or less from the UV opacities, where the  $1 \sigma$  is from the observational uncertainties. Finally, we use the derived dust opacities to infer the intensity and spectral energy distribution of the CIB.

A general characteristic of the model is that galaxies are not a priori closed boxes, but can be experiencing outflows of metal-enriched gas or inflows of metal-free gas. The details of the evolution of each galaxy (e.g., merging, see White & Frenk 1991, versus monolithic collapse, see Ortolani et al. 1995) has little influence on the model, since the computation of the metal and dust fractions does not require assumptions as to the specific characteristics of each galaxy and its interaction with the environment (e.g. presence/absence of merging). To some extent, the infall of small substructures into more massive systems, as predicted in scenarios of hierarchical assembly of galaxies (e.g., Aragon-Salamanca, Baugh & Kauffmann 1998), can be considered similar to gas inflows, although differences may exist as the infalling fragments do not necessarily contain pristine gas. The determination of the dust opacity requires, however, assumptions on the galaxy's mass distribution and on the dust distribution relative to the stars, which we will derive entirely from observational constraints.

### 2.1. Inputs to the Model

### 2.1.1. *The Baryonic Mass in Galaxies*

The total mass locked today in galaxies as stars, planets, dust and gas is calculated to be  $\Omega_{star+gas} \simeq 0.0059 h_{50}^{-1}$  (Gnedin & Ostriker 1992, Fukugita, Hogan & Peebles 1998), or about 10% of the total mass in baryons (Schramm & Turner 1998). Similar numbers can be directly obtained from the local galaxy luminosity function (Marzke, Huchra & Geller 1994). For  $\phi_* = 0.005 h_{50}^3$  and  $L_B^* = 2.4 \times 10^{10} h_{50}^{-2} L_\odot$ , the luminosity density at B in the local Universe is  $L_B \simeq 1.2 \times 10^8 h_{50} L_\odot \text{ Mpc}^{-3}$ ; with an average mass-to-light ratio for the galaxies  $M/L_B = 3.4$ , the average mass density in co-moving space is  $M_{tot} = 4.08 \times 10^8 h_{50} M_\odot \text{ Mpc}^{-3}$ , which is equivalent to the  $\Omega_{star+gas}$  value given above. The average  $M/L_B$  value used in the above calculation is obtained as a weighted mean, assuming that 20% of the galaxies are Ellipticals, with  $M/L_B = 10$  (Worthey 1994), 15% are S0 with  $M/L_B = 5$  and the remaining 65% are spirals and irregulars with  $M/L_B = 1$ .

Kennicutt (1998) measures a typical gas surface density  $\langle \Sigma_{gas} \rangle \simeq 15 M_\odot \text{ pc}^{-2}$  in local spirals. Since the fraction of residual gas in these systems is about 15% of the total baryonic mass, the average surface mass density  $\langle \Sigma_{star+gas} \rangle \simeq 100 M_\odot \text{ pc}^{-2}$ . For the adopted luminosity function and mass-to-light ratio, the average galaxy has total baryonic mass  $M^* = 8.2 \times 10^{10} h_{50}^{-2} M_\odot$ , and the average surface mass density of  $100 M_\odot \text{ pc}^{-2}$  implies a radius of  $16 h_{50}^{-1} \text{ kpc}$ . The resulting virial velocity from this baryon component is  $\sim 150 \text{ km/s}$ . For comparison, in our Milky Way the rotation velocity due to the baryonic component only (disk plus bulge) within its optical radius,  $\sim 12 \text{ kpc}$ , is between  $120$  and  $160 \text{ km s}^{-1}$ , versus a total rotation velocity between  $200$  and  $230 \text{ km s}^{-1}$  due to the combined effect of the baryonic matter and the dark matter halo (Dehnen & Binney 1998).

The local  $\Omega_{star+gas}$  is uncertain by at least 50% (Gnedin & Ostriker 1992, Fukugita et al. 1998), and is one of the parameters in the model with the largest uncertainty.  $\Omega_{star+gas}$  is a lower limit to  $\Omega_{gas}(z = \infty)$  if galaxies undergo gas outflows and, thus, were more massive in the past than today, or it is an upper limit if galaxies experience gas inflows. We note that the presence of metals in the intracluster medium (e.g. Yamashita 1992) strongly favors outflows from galaxies, or a combination of outflows and inflows.

### 2.1.2. *The Stellar Initial Mass Function*

The shape, mass limits, and universality of the stellar Initial Mass Function (IMF) are still matters of heated debate, and choosing an IMF for a model is far from being free of problems. But this is also one of the most crucial steps in the process. The SFR history is presently derived from the measured UV emission of galaxies; the UV emission, however, probes only the light from the most massive stars, and the extrapolation to a SFR density requires adopting an IMF. Most of the mass is locked in stars with mass below  $\approx 1-2 M_\odot$ ; thus the low-mass end of the IMF is the main determinant of the SFR value and, therefore, of the gas consumption rate in galaxies.

Derivations of the high-mass end of the IMF in star-forming regions of nearby galaxies indicate a Salpeter slope above  $\sim 5\text{--}10 M_{\odot}$  and an upper limit of  $100 M_{\odot}$  (Massey et al. 1995, Hunter et al. 1996, 1997), independent of environmental factors, such as metallicity, galaxy type or location within the galaxy. Contrary to the high-mass end, the shape and low mass limit of the IMF below  $\approx 1\text{--}2 M_{\odot}$  is the least known part of the function (see the reviews of Scalo 1998 and Larson 1998). Since most of the light is provided by the most massive stars, direct observations of low mass stars are extremely difficult. Measurements of the IMF in the solar neighborhood and in globular clusters indicate the IMF peaks between  $0.2$  and  $0.5 M_{\odot}$  and has a sharp decline in the number of stars produced below this mass (Kroupa 1995, Scalo 1998). A recent measurement in R136, the central young stellar cluster in the 30 Dor region of the Large Magellanic Cloud, shows that the IMF is Salpeter-like ( $\alpha=2.35$ ) down to  $\sim 2 M_{\odot}$ , and flattens ( $\alpha=1$ ) below that mass (Sirianni et al. 1998). Current uncertainties in the low-mass end of the stellar IMF imply uncertainties in the SFR history up to factors 2–3.

Following the above results, we adopt a Salpeter IMF with a lower cut-off at  $0.35 M_{\odot}$  and an upper cut-off at  $100 M_{\odot}$ . No stars are produced below  $0.35 M_{\odot}$ . The number of stars generated is a factor 1.64 less than for a  $0.1\text{--}100 M_{\odot}$  Salpeter IMF, and a factor 1.55 more than for a  $1\text{--}100 M_{\odot}$  Salpeter IMF. All stars above  $8 M_{\odot}$  explode as supernovae, thus recycling metal-rich gas into the ISM. For our IMF, the return fraction due to supernovae is  $R=0.23$ . For star formation extended over timescales of 1 Gyr or more, the fraction of gas returned to the ISM must include the contribution from stars between  $1$  and  $8 M_{\odot}$ : these stars provide a delayed return of 50% to 80% of the initial mass in form of stellar winds and planetary nebula ejecta. Kennicutt, Tamblyn & Congdon (1994) calculated the contribution of these low-mass stars; their results, normalized to our IMF, imply an effective return fraction  $R_{eff}=0.46$ . Thus, the amount of gas permanently locked into stars over Gyr timescales is  $(1-R_{eff})=0.54$  of the total formed and this effective value is what we adopt in our computation.

### 2.1.3. The Star Formation History

The observed UV emission of galaxies provides the starting point for calculating the history of the SFR density, as the UV light probes the most massive stars and is thus a measure of recent star formation. The UV emission of galaxies has been estimated in the redshift range  $z \simeq 0\text{--}4$  (Lilly et al. 1996, Madau et al. 1996, Connolly et al. 1997). Once an average star formation history and an IMF are assumed for the galaxies, the UV luminosity can be converted into a star formation rate as a function of redshift,  $SFR(z)$  (cf. Madau et al. 1996). The observed UV emission corresponds to different rest-frame wavelengths at different redshifts:  $\sim 2800 \text{ \AA}$  in the range  $0 \leq z \leq 2$  and  $\sim 1500 \text{ \AA}$  for  $z > 2.5$ . For the adopted IMF, which is truncated at the lower end at  $0.35 M_{\odot}$ , a galaxy which is forming stars at a constant rate of  $1 M_{\odot}/\text{yr}$  produces  $1.475 \times 10^{28} \text{ erg s}^{-1} \text{ Hz}^{-1}$  in the UV, with little variation between  $1,500 \text{ \AA}$  and  $2,800 \text{ \AA}$ . The observed  $SFR(z)$ ,  $SFR_{obs}(z)$ , is a *lower limit* to the intrinsic star formation,  $SFR_{int}(z)$ , because of the effects of dust obscuration

mentioned earlier.

A source of uncertainty for the conversion from UV emission to  $\text{SFR}(z)$  is the dependence of the UV emission on the star formation history of the galaxies, especially at longer wavelengths. The flux at  $\lambda < 2000 \text{ \AA}$  is due predominantly to the short-lived  $M > 10 M_{\odot}$  stars and is, therefore, a reasonable estimator of the recent SFR (for a fixed IMF). On the contrary, the UV flux above  $2000 \text{ \AA}$  probes stars with lower and lower masses and becomes more and more sensitive to the star formation history of the galaxy. For instance,  $F(\nu_1)/F(\nu_2) \simeq 1$  for the  $1500 \text{ \AA}$  to  $2800 \text{ \AA}$  ratio for constant star formation,  $F(\nu_1)/F(\nu_2) \simeq 1.5$  for a 1 Myr old instantaneous burst and  $F(\nu_1)/F(\nu_2) \simeq 1$  for a 15 Myr old instantaneous burst. The difference is exacerbated if the burst is lying on top of a pre-existing stellar population (e.g., the residual from previous bursts). Uncertainties in the star formation history, therefore, account for about 30–50% variation (and possibly more) in the conversion UV-to-SFR( $z$ ).

Another source of uncertainty is the potential underestimate of the global UV flux due to incomplete sampling of the lower end of the galaxy luminosity function and, even worse, to uncertain volume corrections. This uncertainty will predominantly affect the high redshift data points, and the point at  $z=4$  in Madau et al. more than the point at  $z=2.75$ . The volume corrections for the UV flux density at  $z=2.75$  are derived from a sample of  $\sim 500$  Lyman-break galaxies with confirmed redshifts (e.g., Steidel et al. 1998, Dickinson 1998; Giavalisco 1998, private communication); thus, for all purposes, we can consider this point as only slightly affected by incompleteness. The UV flux density at  $z=4$ , on the contrary, has been entirely derived from photometric redshifts (B-band dropouts) in two relatively small fields; the  $z=4$  candidate galaxies have not been spectroscopically confirmed yet (except for a handful of recent detections, Dickinson 1998, private communication), so the volume corrections in this case are highly uncertain. Thus, except in one case (see below), we will not attempt to use the  $z=4$  data point as a constraint to the solutions.

#### 2.1.4. *Metals and Dust Production*

Once stars start forming, metal production follows with a negligible time delay, as the first supernovae explode after only 3–4 Myr from the onset of star formation (Leitherer & Heckman 1995). Our emphasis is on the dust content rather than the chemistry galaxies; therefore we adopt here the simplest metal-enrichment scenario, the instantaneous mixing model, to derive metallicities. This model should be adequate to follow the global metal enrichment of galaxies, although it may be insufficient in the case of individual objects (see, e.g., Kunth, Matteucci & Marconi 1995; Tosi 1998). For instantaneous mixing, the relation between the final metallicity of the gas and the fraction of residual gas in the galaxy is given by (Pei & Fall 1995):

$$Z_{gas}(z) = -\frac{\alpha_Z}{1 + \gamma} \ln[M_{gas}(z)/M_{tot}(\infty)]; \quad (1)$$



where  $M_{gas}(z)$  is the galaxy mass in gas at redshift  $z$ ,  $M_{tot}(\infty)$  is the total mass in galaxies at the beginning of star formation,  $\alpha_Z$  is the true yield of the stars, and  $\gamma$  is the outflow parameter;  $\gamma > 0$  implies gas outflows, while  $\gamma = 0$  implies a closed box. The analogous formula for gas inflows is given in Pei & Fall (1995) and is not repeated here. The true yield  $\alpha_Z$  is strongly dependent on the stellar IMF (e.g. Pagel 1987, 1998). Edmunds & Phillips (1997) measure for the global oxygen abundance of galaxies  $[O/H]/[O/H]_{\odot} \sim -0.1$ , which implies a yield  $\alpha_Z \sim 0.7-0.8$  or higher. We adopt  $\alpha_Z = 0.7$  (cf. Table 1); this is an intermediate value between the extremes observed in our Galaxy (Pagel 1987), but we bear in mind that it could be a lower limit, and is uncertain by a factor  $\sim 2$ . This is another difference between our and Edmunds & Phillips' (1997) and Pei & Fall's (1995) approach. We adopt a fixed value for the yield and change the inflow/outflow parameters; the other authors change the yield according to a preselected outflow/inflow parameter. In both cases, however, the target is to constrain the model galaxies to have a predetermined value of the metallicity at  $z=0$ . Equation 1 follows from the assumption that the mass of ejected/accreted gas is proportional to the SFR:  $\delta M_{out/in}(z)/\delta t(z) = \pm \gamma (1 - R_{eff}) \text{SFR}(z)$ , with  $t(z)$  the time corresponding to redshift  $z$  (Pei & Fall 1995). The final metallicity of the gas at zero redshift is here constrained to be  $Z_{gas}(0) = Z_{\odot}$ , the mean gas metallicity of the average  $L^*$  galaxy, with the fraction of residual gas being the observed value of  $\sim 15\%$  (Fukugita et al. 1998).

The initial mass of gas bound in galaxies at  $z=\infty$ ,  $M_{tot}(\infty)$ , is given by the value  $M_{tot}(0) = 4.08 \times 10^8 h_{50} M_{\odot} \text{Mpc}^{-3}$  augmented/decreased by the amount of material ejected into/accreted from the IGM over the history of the galaxy. Thus, the initial mass is given by the formula:

$$M_{tot}(\infty) = M_{tot}(0) \pm \gamma M_{star}(0), \quad (2)$$

where  $M_{star}(0)$  is the total mass in stars at  $z=0$ . As will be discussed in the following sections, a typical galaxy can be expected to eject  $\sim 40\%$  or accrete  $\sim 50\%$  of its initial mass into/from the intergalactic medium (IGM).

Once metals are produced, dust follows within  $\sim 100-200$  Myr (e.g., Tielens 1990, Jones et al. 1994, Dwek 1998). Over the same timescale the dust/metal ratio comes to within a factor  $\sim 2$  of its equilibrium value (Dwek 1998). Studies of local galaxies indicate that the dust/gas mass ratio increases with the metallicity of the gas (Bouchet et al. 1985). Observations of DLAs at redshift  $z \sim 2-3$ , in addition, suggest that the relation between dust/gas and metallicity may not be linear, namely that the conversion from metals to dust may be itself a function of metallicity. In DLAs,  $(\text{dust}/\text{metals})_{DLAs} = 0.5 (\text{dust}/\text{metals})_{MW}$  at  $Z_{gas} \sim 1/15 Z_{\odot}$  (Pettini et al. 1997a). This finding has, however, been challenged by Vladilo (1998), who finds that the  $(\text{dust}/\text{metals})_{DLAs} = 0.6 (\text{dust}/\text{metals})_{MW}$  over the entire metallicity range  $0.1-1 Z_{\odot}$ . Vladilo's result highlights the possibility that DLAs may not be representative of the metallicity evolution of galaxies (see Pettini et al. 1998b). The issue is still open, though, as current samples may select against low-redshift, high-metallicity DLAs if the increasing dust content hampers detection (Boisse' et al. 1998). The theoretical models of Dwek (1998) seem to favor a modestly evolving dust/metals ratio, which goes from  $\sim 1/2$  to its equilibrium value within about 1 Gyr or so,

depending on the star formation history; the same timescale characterizes the slight ( $\sim 50\%$ ) overabundance of silicate dust over carbon dust when low mass stars have not evolved yet. As a working hypothesis, our model contains a quadratic relationship between the dust/gas ratio and the metallicity, normalized to match the observed DLAs value at  $Z_{gas}=1/15 Z_{\odot}$ , and the Galactic value dust/gas=0.0056 at  $Z_{gas}=Z_{\odot}$ . The quadratic relation does not necessarily reflect the actual dust enrichment of galaxies, but it is the simplest possible formulation given the poor constraining the observations currently provide. We will discuss later the consequences of relaxing this assumption.

### 2.1.5. The Dust Opacity

The dust opacity of a galaxy is determined by the combination of three ingredients: 1. the dust column density; 2. the extinction curve; 3. the geometrical distribution of the dust in the galaxy.

The simplest formulation for the dust column density  $E(B-V)$  is:

$$E(B - V) \propto N(H) \times F(Z) \quad (3)$$

where  $N(H)$  is the gas column density, and  $F(Z)$  is the quadratic function of the metallicity defined in section 2.1.4 for the dust/gas ratio.  $F(Z)$  describes the fact that low metallicities imply dust/metals ratios lower than the Galactic value (Pettini et al. 1997a). The proportionality constant is the Galactic conversion factor between  $N(H)$  and  $E(B-V)$  ( $E(B-V)=N(H)/5.9E+21$ , Bohlin, Savage & Drake 1978). The average gas column density  $N(H)$  is proportional to the fraction of residual gas in the galaxy and to the galaxy surface mass density. The fraction of residual gas is given by the balance between star formation, gas recycling, and outflows/inflows. The average surface mass density at  $z=0$  (section 2.1.1),  $\Sigma_{star+gas}(0) \simeq 100 M_{\odot} \text{ pc}^{-2}$ , is a lower/upper limit to the surface mass density at higher redshift, if outflows/inflows are present. In sections 3 and 4, we will see that  $\Sigma_{star+gas}(z)$  is a factor  $\sim 1.7(2.0)$  higher(lower) at  $z=10$  than at  $z=0$  in case of outflows(inflows).

In order to infer the behavior of the average surface mass density  $\Sigma_{star+gas}(z)$  as a function of redshift, we use the observational properties on the largest sample of high redshift galaxies available to-date: the Lyman-break galaxies (cf. Steidel et al. 1996). These  $z\sim 3$  galaxies have median 1500 Å luminosity  $L_{1500}=6.3\times 10^{40} \text{ erg s}^{-1}$  within the half-light radius (Steidel et al. 1996) and angular half-light radii around  $0''.2-0''.3$  (Giavalisco et al. 1996, 1998), the latter corresponding to physical half-light radii of  $1-3 h_{50}^{-1} \text{ kpc}$  for a large range of values of  $q_o$ . The bolometric surface brightness within the half-light radius is then  $SB\approx 2.1\times 10^9 L_{\odot} \text{ kpc}^{-2}$ , and the dust attenuation corrected surface brightness is  $SB\approx 6-12\times 10^9 L_{\odot} \text{ kpc}^{-2}$  (Pettini et al. 1998a, Calzetti 1997). If star formation has been constantly active for 0.5–1 Gyr (cf. Pettini et al. 1998a), the mass-to-light ratio is  $M/L=0.015-0.025$ , and the average stellar surface mass density of the Lyman-break galaxies is in the range  $90-300 M_{\odot} \text{ pc}^{-2}$ . To this, we have to add the surface mass density of

the gas. Technically, at  $z=3$  more than 90% of the mass is still in gas, but a lower fraction could be present in the Lyman-break galaxies if they are going through a major star-formation event. We ascribe to the  $z=3$  galaxies the conservative figure of  $\sim 50\%$  gas fraction, implying a total surface mass density  $180\text{--}600 M_{\odot} \text{ pc}^{-2}$ . The  $\Sigma_{star+gas}(z)$  of the Lyman-break galaxies is thus a factor up to 3, 6, 10 higher than the instantaneous value predicted at  $z=3$  by outflows, closed-box, inflows, respectively; it is also a few times higher than local value  $\Sigma_{star+gas}(0) \simeq 100 M_{\odot} \text{ pc}^{-2}$ . In addition, the observed half-light radii of the Lyman-break galaxies are on average a factor  $\sim 2$  smaller than the half-light radii of local galaxies, which range between 3 and 6 kpc. The evolution of the surface mass density and of the half-light radius between  $z=3$  and  $z=0$  can be due to one of two reasons: (1) Lyman-break galaxies are fragments of galaxies which will merge into larger units and are undergoing intense star formation (Lowenthal et al. 1997); (2) Lyman-break galaxies are massive galaxies (Steidel et al. 1996) and stellar formation is proceeding “inside-out”. In the latter case, larger surface mass densities and smaller radii at high redshift are explained by the fact that star formation is concentrated in the central regions of the galaxies, where the density is higher. Whichever the reason, we use the observational results to model the evolution of the effective surface mass density as a monotonically increasing function of redshift relative to the instantaneous value implied by the presence of outflows/closed-box/inflows at the same redshift. We have only two points to tie the evolution to, one at zero redshift and the other at  $z\sim 3$ , and little handle on the driving physical parameters. In first approximation, we assume that the evolution is driven by the fraction  $f_{gas}$  of residual gas in the galaxy, in the range  $0.5 < f_{gas} < 1$ . Figure 1 shows our parametrization of the evolution of the ratio of the effective to instantaneous surface mass densities  $\Sigma_{star+gas,eff}(z)/\Sigma_{star+gas,inst}(z)$ . For instance, the outflow/closed-box/inflows models of section 3 give  $\Sigma_{star+gas,inst}(3)=155/100/75 M_{\odot} \text{ pc}^{-2}$  due to the presence/absence of outflows/inflows of gas, implying  $\Sigma_{star+gas,eff}(3)=420/270/200 M_{\odot} \text{ pc}^{-2}$ . We stress that the “extra” evolution of the surface mass density implied by  $\Sigma_{star+gas,eff}(z)/\Sigma_{star+gas,inst}(z)$  is purely observational. Gas fractions  $f_{gas} < 0.5$  generally correspond to redshift  $z \leq 1$ , and we assume that at this stage the effective surface mass density is identical to its instantaneous value. This assumption of no-evolution for  $z \leq 1$  is supported by the Medium Deep Survey galaxy sample of Phillips et al. (1995); the sample has median redshift  $z \simeq 0.3$ , and the galaxies show no evolution of either the half-light radius or of the disk-to-total ratio.

The effective dust column density thus evolves as:

$$E(B - V)_{eff} \propto N(H) \times F(Z) \times \frac{\Sigma_{gas+star,eff}(z)}{\Sigma_{gas+star,inst}(z)}. \quad (4)$$

As extinction curve, we adopt the Small Magellanic Cloud curve (Bouchet et al. 1985), which is currently the only one known for a low metallicity ( $Z \simeq 0.1 Z_{\odot}$ ), star-forming galaxy; we adopt this curve as the best available for describing high redshift galaxies. The choice of an extinction curve is important only for  $\lambda < 2800 \text{ \AA}$ ; at redder wavelengths, the three known mean extinction curves (Galactic, LMC, and SMC, see, e.g., Fitzpatrick 1986) give similar attenuation values to within 5% for a mixed geometry (see below) and for  $E(B-V) \leq 2$ , well within the parameter space

we explore.

When dealing with galaxies as a whole, the simplest geometry is a homogeneous mixture of dust, gas, and stars (Witt et al. 1992). This has been shown to be valid in the low redshift regime for disk galaxies (Xu & Buat, 1995, Wang & Heckman 1996), and for starburst galaxies when the underlying old stellar population is considered together with the young starburst population (Buat & Burgarella 1998). Whether this is true in the high redshift regime, where all stellar populations are young and the entire galaxy may be acting as a single starburst region (Calzetti 1997a, Meurer et al. 1997), is not clear. We will assume in first approximation the mixed geometry to be valid at all redshifts. Among the solutions presented in section 3, one case (Model 5) will have this assumption relaxed for high redshift galaxies; other geometries will be discussed in section 4.2. Observations of local galaxies indicate that the ratio of the scale heights of stars and dust is a function of the wavelength. In particular, the stars responsible for the UV emission of a galaxy have the same scale height as the dust,  $h_{star,UV}=h_{dust}$  (e.g. Wang & Heckman 1996), while the optical emission from a galaxy is generally more vertically extended,  $h_{star,opt} \simeq 2-4 h_{dust}$  (e.g., Kylafis & Bahcall 1987). This is in agreement with the general result that dust is mostly concentrated in the arms of spiral galaxies, where star formation is occurring (White, Keel, & Conselice 1997, Gonzalez et al. 1998). We adopt two different functional behaviors for the ratio  $h_{star}/h_{dust}$  (Figure 2): one (hh1) which varies from 1 in the UV to 2 at I, with a sharp change happening in the B band, and the other (hh2) smoothly changing from 1 at 1,000 Å to 4 at I. Both functional behaviors are used throughout this paper. Finally, we are modelling galaxies as flattened mass distributions and the final ‘net’ opacity (absorbed-to-total light ratio) is obtained from the average of the model galaxy over all inclination angles. The formalism for the thin disk opacity model is detailed in Wang & Heckman (1996). The thin disk approximation does not take into account that nowadays about 1/3 of the galaxies are pure spheroids (ellipticals and S0s) and contain about twice the mass of spirals (Persic & Salucci 1992, see also Schechter & Dressler 1987 and Fukugita et al. 1998). We will neglect this fraction because: (1) high-mass star formation nowadays appears concentrated in flattened distributions (Scoville et al. 1998, Downes & Solomon 1998) and we are mostly interested in the opacity suffered by the UV emission from massive stars; (2) the fraction of spheroids may not be constant in time; Kauffmann, Charlot & White (1996) suggest that only 1/3 of the present-day spheroids are assembled at  $z \sim 1$ . If galaxies were formed by hierarchical merging of substructures, this may indeed have occurred late in the life of the Universe, at  $z \leq 1$ , and most of the high-redshift star formation is occurring in disk-like structures (Kauffman 1996, Baugh, Cole & Frenk 1996). The presence of spheroids, in addition, has little effect on the final average over the inclination angles: we estimate that for  $h_{star}/h_{dust}=1$  and  $E(B-V) \leq 1$  the ‘net’ opacity decreases by a factor  $\sim 1.25$  if we allow for a mixture of 2/3 flattened disks and 1/3 spheroids.

### 2.1.6. The Dust Emission

The fraction of stellar light absorbed by dust at UV and optical wavelengths is re-emitted in the FIR. In order to calculate the intensity and spectrum of the dust FIR emission, we need to assume a spectral energy distribution for the galaxy’s stellar population and a model for the dust emission.

We adopt for the stellar population a 1 Gyr old continuous star formation SED with solar metallicity (Bruzual & Charlot 1996). The dependence of the FIR emission on the age of the stellar population is negligible for the constant star formation case, because the FIR flux receives the bulk of the contribution from the UV emission of the stars. However, the 1 Gyr population will generally be too blue at optical wavelengths in the latest stages of the Universe, as in our cosmology the Universe today is 13.3 Gyr old. Thus, for sake of completeness, we will also show in section 4.2 the case of a 5 Gyr continuous star formation population. Whichever the model adopted for the galaxy SED, the UV spectrum is normalized to the observed luminosities. The normalization is from the observed flux density at 2,800 Å in the range  $z=0-1$  (Lilly et al. 1996), after the model SED is convolved with the opacity at the same wavelength. The fraction of ionizing photons absorbed by dust is given by the formula reported in Calzetti et al. (1995). Despite the low metallicity SEDs being generally bluer than the high metallicity SEDs, the decreasing average metallicity at higher redshift has a relatively minor impact on the average galaxy SED, on the basis of current population synthesis models. The difference in the number of ionizing photons for metallicities between 0.1 and twice  $Z_{\odot}$  is about 13%, and the difference in the normalized UV flux is about 11% (Leitherer & Heckman 1995).

The dust emission spectrum is by no mean well known or easily parametrized in local galaxies. Our Milky Way shows a complex combination of blackbody temperatures (Cox, Krügel & Mezger 1986, Désert, Boulanger & Puget 1990), and other galaxies as well are better described by multiple temperature components, with the most simplified models using at least two (Lonsdale-Persson & Helou 1987, see also the ISO data of Krugel et al. 1998). For the purpose of this study we consider the simplest possible case: a single-temperature blackbody distribution convolved with a dust emissivity  $\propto \nu^{\epsilon}$ , where  $\epsilon = 2$ , bearing in mind that this is an oversimplification. The temperature of the dominant dust emission component is correlated with the star formation activity in low redshift galaxies (Helou 1986); in starburst galaxies, the observed correlation is between the temperature and the FIR surface brightness of the star forming region (Lehnert & Heckman 1996), implying a correlation between temperature and the surface density of the star formation. We reproduce this trend for the dust temperature with:

$$T(z) \propto \left( SFR_{int}(z) \frac{\Sigma_{star+gas,eff}(z)}{\Sigma_{star+gas,inst}(z)} \right)^{1/(4+\epsilon)}, \quad (5)$$

where  $T(z)$  is the blackbody temperature as a function of redshift and  $SFR_{int}(z)$  is the intrinsic star formation rate;  $\Sigma_{star+gas,eff}(z)/\Sigma_{star+gas,inst}(z)$  measures how “concentrated” the star formation is and has value  $\approx 3$  at  $z=3$  (see section 2.1.5 and Figure 1).  $SFR_{int}(z) \Sigma_{star+gas,eff}(z)/\Sigma_{star+gas,inst}(z)$

is a measure of the surface star formation density, and, thus, of the surface brightness of the star forming region. The proportionality constant for Equation 5 has been chosen to recover the mean dust temperature of local quiescent galaxies ( $T \sim 20$  K).

## 2.2. Outputs from the Model

The three main outputs from this model of galaxy evolution are:

1. the intrinsic SFR density as a function of redshift; this is the result of the iterative process to yield consistent solutions between the dust opacities and the correction factors to the UV-derived global SFR density;
2. the dust opacities, defined as the fraction of emerging to total stellar light, at UV and blue wavelengths (galaxy restframe) as a function of redshift;
3. and the spectral energy distribution of the CIB in the range 100–2,000 $\mu$ m (observer’s restframe), from the integral along the line of sight of the dust emission from galaxies.

These outputs are compared with available data. The strongest constraints come from observations of the Local UV opacity (e.g., Wang & Heckman 1996), from the H $\alpha$ - and ISO-derived intrinsic SFR density at low redshift (Gronwall 1998, Hammer & Flores 1998), and from the measured CIB from COBE DIRBE and FIRAS (Hauser et al. 1998, Fixsen et al. 1998). Predictions from intermediate steps of the model, namely the evolution of the metal content, of the gas column density, and of dust temperature, and the local FIR energy density are also compared with available observational data.

## 3. Results

Galaxy evolution is first followed by using the observed SFR( $z$ ) as star formation history (Model 1, see Figure 3). The main properties of the model are listed in Table 1. The observed SFR( $z$ ) is unable to reproduce the basic characteristics of the local Universe: the amount of stars produced by  $z=0$  is  $\Omega_{star} = 0.0012 h_{50}^{-1}$ , or 24% of the total stellar mass observed today in galaxies. The residual gas fraction at  $z=0$  is 80%, well above the local value of 15%, and, as consequence, the final metallicity of the gas is about 1/6  $Z_{\odot}$ . The final metallicity of Model 1 is so much below solar that outflows/inflows are not required to regulate it, and galaxies have been treated as closed boxes. To create a reference baseline, the surface mass density has been assumed non evolving,  $\Sigma_{gas+star,eff}(z)/\Sigma_{gas+star,inst}(z)=1$ . From the simple act of forming stars, Model 1 predicts non-zero opacities. In particular the emerging 2800 Å and 1500 Å fluxes from galaxies at  $z \leq 0.1$  are about 1/2 and 1/3 of the total, respectively (Figure 4). Thus, despite the small final metallicity, the low redshift opacities are relatively large; this is due to the large

residual gas fraction. The presence of non-zero UV opacities is, of course, in contradiction with the assumption that the observed, UV-derived  $\text{SFR}(z)$  is equivalent to the intrinsic  $\text{SFR}(z)$ , namely  $\text{SFR}_{obs}/\text{SFR}_{int}=1$ . The magnitude of the contradiction is shown in Figure 4 itself, where  $\text{SFR}_{obs}/\text{SFR}_{int}$  is compared with the predicted emerging-to-total light at the appropriate wavelength. The FIR background implied by those opacities (Figure 5) is  $\leq 25\%$  of the observed values from COBE DIRBE+FIRAS results. This comparison, although necessary for sake of clarity, is artificial, because by assumption Model 1 does not contain dust, and therefore there cannot be a CIB. As a general consideration, Model 1 produces far too little mass permanently locked in stars; even an IMF with a Salpeter slope down to  $0.1 M_{\odot}$  would only produce a factor 1.64 more mass in stars. Thus the star formation rates must be higher than directly measured.

The predicted UV opacities of Model 1 provide guidelines for the iterative procedure to produce self-consistent corrections to  $\text{SFR}_{obs}$ , the observed  $\text{SFR}(z)$ . The solution the procedure converges to is not unique; with our limited knowledge of  $\text{SFR}_{obs}$ , which consists of 6 observational data points (i.e., excluding the  $z=4$  one), we find two solutions (Model 2 and Model 3) to  $\text{SFR}_{int}$ , when we allow for either closed-box or outflow models. The case of inflows is also discussed (Model 4), but less extensively, because the solution is somewhat intermediate between Model 2 and Model 3. In a fourth solution (Model 5), we impose the  $\text{SFR}_{obs}$  point at  $z=4$  to be a constraint, and we also allow for variation of some of the input parameters. Model 2 and Model 3 bracket two extreme behaviors of the intrinsic  $\text{SFR}(z)$ , for the selected input parameters. However, as we will see in the next section, one of the two satisfies the available observational constraints better than the other, within the limits of our assumptions. All Models allow the effective surface mass density of galaxies to evolve with the residual gas fraction  $f_{gas}$  (see Figure 1). The main characteristics of the four solutions are summarized in Table 1.

The  $\text{SFR}_{int}$  of Model 2 (Figure 3) dictates that star formation increases from  $z=10$  (our fiducial starting point for star formation) to  $z \simeq 1.2$ , and then decreases from  $z \simeq 1.2$  to the present. The global shape is similar to  $\text{SFR}_{obs}$ , but the correction factors are different at high and low redshift. In particular, at  $z=2.75$   $\text{SFR}_{int}=1.8 \times \text{SFR}_{obs}$ , while at  $z < 1$   $\text{SFR}_{int}=3.9 \times \text{SFR}_{obs}$ ; galaxies are, therefore, more opaque at recent times than at high redshift. As mentioned earlier we do not attempt to use the  $\text{SFR}_{obs}$  at  $z=4$  as a constraint either in this Model or in Models 3 and 4. The final metallicity of Model 2 is  $3/4 Z_{\odot}$ , implying that excess metals are not produced; thus galaxies are treated as closed boxes. The residual gas fraction at  $z=0$  is  $f_{gas}=0.34$ ; this value is larger than the target of 15%, but we consider it marginally acceptable in view of the large uncertainties affecting each of our input parameters. The mass in stars is 78% of the target value. The dust column density is an increasing function of time and a similar behavior is displayed by the opacities (Figure 6). The predicted  $2800 \text{ \AA}$  emergent-to-total radiation in the local Universe is around a factor 0.24 (Figure 7). Such high dust opacity at low redshift implies comparably low redshifts for the main contributors to the CIB radiation; Figure 6 shows the contribution to the flux of the CIB as a function of redshift: most of the contribution to the observer’s restframe emission at  $140 \mu\text{m}$  comes from galaxies at  $z \sim 1$ , while the contributors to the  $240 \mu\text{m}$  emission are more smoothly

distributed with median redshift  $z \sim 1.4$ . At longer wavelengths, the flux contribution to the CIB is smoothly distributed at redshift  $z > 1$ , and is almost constant at  $850 \mu\text{m}$ . The dust temperature peaks at  $z \sim 1.2$ , following the shape of  $\text{SFR}_{int}$  (see Equation 5). Model 2 agrees with observations of the CIB at short wavelengths ( $\lambda < 400 \mu\text{m}$ ), but falls short of the data at longer wavelengths (Figure 8); the predicted FIR SED is thus too hot in comparison with data, in agreement with the hottest galaxies being located at relatively small redshift (Figure 6).

The second solution which satisfies the self-consistency requirement between  $\text{SFR}_{obs}/\text{SFR}_{int}$  and the UV opacities is shown in Figures 9 to 11 (Model 3). The  $\text{SFR}_{int}$  of Model 3 is completely different from Model 2 (Figure 3): it is constant at high redshift and decreases below  $z \sim 1.2$ , roughly resembling the  $\text{SFR}(z)$  of Rowan-Robinson et al. (1997). In numbers: at  $z = 2.75$   $\text{SFR}_{int} = 5.8 \times \text{SFR}_{obs}$  and at  $z \leq 1.2$   $\text{SFR}_{int} = 3.2 \times \text{SFR}_{obs}$ . In Model 3, the residual gas fraction at  $z = 0$  is 13%, practically meeting the target of 15%. The large amount of star formation implies that outflows are invoked to maintain the final gas metallicity in galaxies to solar values; thus galaxies were on average 1.7 times heavier at  $z = 10$  than at  $z = 0$  (cf. Edmunds & Phillips 1997), and  $\Omega_{gas} = 0.0082$  at  $z = 3$ . The resulting rotation velocities at  $z = 3$  are  $\sim 250 \text{ km s}^{-1}$ , for a constant mass in dark matter and for a local typical rotation speed of  $210 \text{ km s}^{-1}$ , thus still perfectly reasonable. In the absence of outflows, the final metallicity of the galactic gas would be  $Z = 1.44 Z_{\odot}$ . The dust column density peaks at  $z \sim 1.8$  (Table 1 and Figure 9), due to the decreasing gas fraction despite the still increasing metallicity of the galaxy; the ratio of the emerging-to-total light from galaxies follows an analogous trend. This trend is in agreement with the correction factors applied to  $\text{SFR}_{int}$  (Figure 10), as expected from the fact that Model 3 is a solution to our iterative procedure. The large opacities at high redshift imply that the contributors to the CIB in Model 3 are spread over a larger redshift range than in Model 2 (Figure 9). The peak of the contribution at  $140 \mu\text{m}$  is around  $z = 1.2$ , not very different from Model 2, but the contribution to the  $240 \mu\text{m}$  CIB emission is spread over the entire redshift range sampled, with a median at  $z \sim 2.4$ . Even more extreme is the redshift dependence of the flux contributions at  $450 \mu\text{m}$  and  $850 \mu\text{m}$ , which increase with  $z$ . The predicted FIR background is given in Figure 11, where it is compared with the observed CIB results. The agreement between the CIB data and the prediction of Model 3 is much better than in Model 2, and is within the  $1 \sigma$  error bar of the observations for the entire spectral range up to  $1600 \mu\text{m}$ . The Model 3 spectrum still tends to be slightly hotter than the observational points at the longest wavelengths. However, the long wavelength regime is also the region where the FIRAS data have the largest uncertainties, thus it is hard to estimate the real disagreement between model and data.

When inflows of metal-free gas, rather than outflows of metal-rich gas, are invoked to constrain the metallicity of the galactic gas to solar values at  $z = 0$ , the iterative procedure converges to a solution (Model 4) intermediate between Model 2 and Model 3 in the low- $z$  regime and close to Model 3 in the high- $z$  regime. In Model 4,  $\text{SFR}_{int} = 3.5 \times \text{SFR}_{obs}$  at  $z < 1$ , and  $\text{SFR}_{int} = 4.4 \times \text{SFR}_{obs}$  at  $z = 2.75$  (Figure 3). The final gas fraction here is  $f_{gas} = 0.19$ , very close to the target value; without inflows the final metallicity would be  $Z = 1.17 Z_{\odot}$ , slightly above solar. The initial mass



in galaxies at  $z=10$  is a factor 0.68 of the local value, and  $\Omega_{gas}=0.0035$  at  $z=3$ . The dust column density peaks at  $z=0.4$  (Figure 12), and the opacities follow the same trend; the result of the iterative procedure can be seen in Figure 13, where the ratio  $SFR_{obs}/SFR_{int}$  is shown to match the emerging-to-total UV light. Model 4 reproduces the CIB observations with a similar level of accuracy as Model 3 (Figure 14), thanks to the large UV opacities at high- $z$ .

For the solution Model 5 (see Figure 3 and Table 1), the value of  $SFR_{obs}$  at  $z=4$  is used as an additional constraint. In this model, we also explore the effect of changing some of the input parameters. The true yield  $\alpha_Z$  is increased from 0.7 to 1.0, the latter being possibly closer to the actual yield of stars. The stellar populations in high- $z$  ( $z \geq 2.75$ ) galaxies are completely embedded in, rather than uniformly mixed with, dust, possibly a better representation of primeval galaxies. Finally, we assume that the dust/metal ratio does not evolve, but is a constant equal to the Milky Way value. The effect of these assumptions is shown in Figure 15: the peak of the dust column density is much higher, by a factor  $\geq 3$ , than in the other three models, clearly reflecting the effect of the larger amount of metals produced (higher  $\alpha_Z$ ) and of the larger fraction of dust created (dust/metals=constant). The match between the  $SFR_{obs}/SFR_{int}$  ratio and the emergent-to-total UV light (Figure 16) is achieved by producing 111% of the target mass in stars and leaving only 6% of residual gas. Even so, the agreement between  $SFR_{obs}/SFR_{int}$  and the emergent-to-total light is not as good as in the three previous cases: a better match would require an increase of  $\sim 10\%$  of the  $SFR_{int}$  at  $z < 1.2$ ; this is however problematic because the model would immediately run out of gas. The large amount of metals produced requires large outflows to constrain the final metallicity of the galaxy to  $Z_{\odot}$ : the initial baryonic mass in galaxies needs to be 4 times larger than at  $z=0$ . In the absence of outflows the final gas metallicity would be  $Z=2.90 Z_{\odot}$ . Model 5 does not reproduce the spectral energy distribution of the CIB as well as Models 3 or 4 (Figure 17). However, the discrepancy between predictions and data in Figure 17 disappears almost completely if we change the dust emissivity index from  $\epsilon=2$  to  $\epsilon=1.5$ .

The mixed dust/star geometry adopted in Models 2–4 and in the low redshift regime of Model 5 produces a grey effective extinction, namely, a mild reddening coupled with large global attenuations. This is a general characteristic of mixed geometries (Witt et al. 1992); its effect is shown in Figure 18, where the attenuation at the peak column density  $E(B-V)_p$  for each of the four Models (Table 1) is compared with the extinction produced by a foreground screen of dust with an SMC curve and a modest  $E(B-V)=0.1$ . The reddening between 1000 Å and 10000 Å produced by  $E(B-V)_p \sim 0.3$  in Models 2–4 is comparable with the case of a foreground screen with  $E(B-V)=0.1$ , but the global attenuations are a factor  $\sim 1.5$  larger. As a result, the galaxies in our model Universe will appear blue, even in the presence of non negligible dust obscuration. Model 5 stands out from the general trend of the other three models because its input parameters dictate larger global dust column densities.

In the next section, we will concentrate the discussion on the differences between Model 2 and Model 3, which represent two extreme behaviors. We recall Model 4 only when needed for completeness, as the general behavior of the latter is relatively close to Model 3. The same will be

done for Model 5, although this solution implies rather extreme conditions at  $z < 1$ , in the form of large opacities.

## 4. Discussion

### 4.1. The Intrinsic Star Formation History

Models 2 and 3 imply drastically different star formation histories for the Universe, although they are both reasonable solutions for our model of galaxy opacity evolution (Figures 7 and 10). In Model 2, 34% of the star formation happens at redshift  $z \geq 1.2$ , and only 2% of the stars are produced at  $z > 3$ . In Model 3, 57% of the star formation happens at redshift  $z \geq 1.2$ , with 20% of the stars produced at  $z > 3$ . The difference between the two models is even more obvious when redshifts are converted in time, since Model 2 and Model 3 imply that 1/3 and more than 1/2, respectively, of the star formation happened during the first  $\sim 4$  Gyr since the beginning of the Universe (for our adopted cosmology). For comparison, Model 5 produces 1.5% of the total mass in stars at  $z > 3$  and 45% at  $z \geq 1.2$ .

Model 2, however, reproduces the CIB spectral energy distribution less accurately than Model 3 (cf. Figure 8 with Figure 11). Model 2 would not necessarily be in better agreement with the CIB if a value of the dust emissivity  $\epsilon < 2$  were adopted, especially if we consider a more realistic model of the galaxies FIR emission. Local galaxies are characterized by a broad distribution of dust temperatures, of which our assumed  $T = 20$  K is most likely towards the low end of the range. Local galaxies have a FIR distribution skewed towards higher energies and spread over a larger range of frequencies than assumed here, with peaks around wavelengths  $\leq 140 \mu\text{m}$  (e.g., Krugel et al. 1998). Even if  $\epsilon$  is less than 2 in actual galaxies, this does not guarantee that the global emission will have more power at long wavelengths, because of the broad FIR energy distribution. Most likely, Model 2 will still be unable to reproduce the CIB at long wavelengths.

As discussed in the previous section, Models 2 and 3 predict different redshift dependences of the flux contribution to the CIB at long wavelengths. For instance, Model 2 gives a rather flat 850  $\mu\text{m}$  contribution for  $z > 1$  (cf. Figure 6), while in Model 3 the contribution is an increasing function of redshift. More in detail,  $\langle \text{Flux}(850, 2 < z \leq 5) \rangle = 3.55 \langle \text{Flux}(850, 0.9 \leq z \leq 2) \rangle$  in Model 3 and  $\langle \text{Flux}(850, 2 < z \leq 5) \rangle = 0.92 \langle \text{Flux}(850, 0.9 \leq z \leq 2) \rangle$  in Model 2. The redshift range  $2 < z \leq 5$  spans a time interval of 1.7 Gyr, while  $0.9 \leq z \leq 2$  spans an interval of 2.5 Gyr. Since we assume that the number density of galaxies is a constant, such differences in background flux are due to variations in the total FIR luminosity of the sources in the band. In Model 3, where the SFR density is constant for  $z > 1$ , the flux contribution to the the 850  $\mu\text{m}$  band is determined by the slight increase of the dust temperature with redshift and the k-correction within the band. For Model 2, the contribution to the 850  $\mu\text{m}$  is a combination of k-corrections and both variable  $\text{SFR}_{int}(z)$  and  $T(z)$ . The SCUBA sources, which sample the bright end of the FIR luminosity function, should be mostly located at  $z > 2$  if Model 3 is correct, or be roughly homogeneously

distributed as a function of redshift if Model 2 is correct. The current (uncertain) redshift placements give 3–5 sources at  $0.9 \leq z \leq 2$  and 8–10 sources at  $z > 2$  (depending on where we place the two sources of Barger et al. 1998), implying a ratio 1.6–3.3 with a median value of  $\sim 2.3$  between the two redshift bins. The result is still inconclusive, and must await further constraints on the redshifts of the sources. For reference, the reddest (dustiest)  $z \sim 3$  Lyman-break galaxies in the Hubble Deep Field are below the detection limits of the SCUBA observations; their predicted fluxes are below 1.7 mJy and mostly around  $\sim 1$  mJy (Meurer et al. 1998), while the SCUBA-HDF field has a  $5 \sigma$  detection limit of 2 mJy (Hughes et al. 1998).

As mentioned in Section 2.1.3, the  $SFR_{obs}$  data point at  $z \sim 4$  has not been used as a constraint for Models 2–4 due to the potential underestimate introduced by incompleteness and volume corrections. A posteriori, we can infer that Model 2 implies that the observed  $z \sim 4$  point should be underestimated by a factor  $\sim 1.5$ , while Models 3 and 4 imply that this data point is underestimated by a factor  $\sim 3$ .

We now compare the predicted  $SFR_{int}$  for the local Universe (Models 2 to 5) with the results of observational surveys in  $H\alpha$  or radio, which are less sensitive to dust obscuration than the UV emission. All our solutions give the local  $SFR_{int}$  between a factor 3 and 4 of the value measured from UV observations, namely  $SFR_{int} = 0.0095\text{--}0.0125 M_{\odot} \text{ yr}^{-1} \text{ Mpc}^{-3}$  at a median redshift of 0.05, with the lowest value given by Model 3. The local ( $z < 0.05$ ), reddening-corrected  $H\alpha$  luminosity density of Gronwall (1998) corresponds to an intrinsic  $SFR = 4.1 \times 10^{-42} L(H\alpha) \sim 0.008 M_{\odot} \text{ yr}^{-1} \text{ Mpc}^{-3}$  for our IMF; the analogous data point from Gallego et al. (1995) gives  $SFR \sim 0.005 M_{\odot} \text{ yr}^{-1} \text{ Mpc}^{-3}$ . The data points carry a typical uncertainty of  $\sim 50\%$  (e.g., Gallego et al. 1995). Radio observations of local galaxies trace the supernova rate and, indirectly, the star formation rate at a wavelength which is not affected by dust obscuration; the SFR density inferred from observations at 1.4 GHz is  $\sim 0.016 M_{\odot} \text{ yr}^{-1} \text{ Mpc}^{-3}$  on our IMF scale, again with  $\sim 50\%$  uncertainty (Cram 1998). Therefore, our  $SFR_{int}$  is in reasonable agreement with the data points from both  $H\alpha$  and radio observations.

Another important check is whether the amount of dust implied by our solutions overpredicts the FIR emission from local galaxies, the latter being measured by IRAS. The FIR emissivity at  $60 \mu\text{m}$  in the local ( $z < 0.01$ ) Universe is  $\nu F(\nu) \simeq 3.4 \times 10^7 L_{\odot} \text{ Mpc}^{-3}$  (Villumsen & Strauss 1987, Soifer & Neugebauer 1991). The total FIR energy density in the wavelength range 8–1000  $\mu\text{m}$  from our Models 2–4 is  $E(8\text{--}1000 \mu\text{m}) \simeq 6.9\text{--}9.3 \times 10^7 L_{\odot} \text{ Mpc}^{-3}$  at the same median redshift. Using a conversion factor of 2.67 between total energy and power at  $60 \mu\text{m}$  (cf. Soifer & Neugebauer 1991), the predicted total FIR emissivities in the models correspond to predicted  $60 \mu\text{m}$  emissivities of  $\sim 2.6\text{--}3.5 \times 10^7 L_{\odot} \text{ Mpc}^{-3}$ , which bracket the observations.

Infrared observations also offer an independent measure of the intrinsic SFR density of the Universe. ISO observations at  $6.75 \mu\text{m}$  and  $15 \mu\text{m}$  of one of the CFRS fields have been recently used to derive preliminary values of the SFR over the redshift range  $0.3 \leq z \leq 1$  (Hammer & Flores 1998). The  $SFR_{int}$  of Models 2 and 3 are a factor  $1.7 \pm 0.25$  and  $1.4 \pm 0.2$ , respectively, larger

than the ISO values in the same redshift range. The difficulty with this type of observations is in the uncertain derivation of a SFR from the restframe  $\sim 10 \mu\text{m}$  emission of galaxies. However, if confirmed by further data, the excess  $\text{SFR}_{int}$  at low- $z$  given by our solutions may imply that either our galaxy model is too simplistic in the low redshift regime, where the dust is mixed with multiple-age populations; or that the intrinsic SFR at high redshift is even higher than what required by Model 3.

Relatively low UV opacities at  $z < 1$  require, indeed, a high gas consumption rate at high redshift, namely high  $\text{SFR}_{int}$ . The average dust column density of a galaxy,  $E(B-V)$ , is the result of two opposite effects, both monotonically dependent on time: increase in metallicity, which increases  $E(B-V)$ , and decrease of the gas fraction, which decreases  $E(B-V)$ . The peak at  $z \simeq 1.8$  for the dust column density in Model 3 is a consequence of those opposite processes. Low opacities at  $z < 1$  thus require that a large fraction of the gas has been already locked in stars. For this to happen,  $\text{SFR}_{int}$  at high redshift must be large, which also induces a faster metal enrichment of the galaxy’s ISM, like in Model 3. As a result, high- $z$  galaxies will tend to be opaque. The UV attenuation  $A_{1500} = 1.85$  mag predicted by Models 3 and 5 at  $z=3$  is in agreement with the recent results by Pettini et al. (1998a), who find attenuation values  $A_{1500} \simeq 1-2$  mag in six Lyman-break galaxies, from joint measurements of rest-frame UV spectra and optical nebular line emission.

Various authors (e.g. Dickinson 1998, Meurer et al. 1997, Calzetti 1997a, Pettini et al. 1998a) have attempted to correct the UV emission of the Lyman-break galaxies at  $z=3$  using the ‘starburst’ reddening curve derived by Calzetti et al. (1994). In particular, the UV spectra of these galaxies appear reddened by a color excess  $E(B-V) \sim 0.15$  if the functional shape of Calzetti (1997a) is used. We have plotted in Figure 19 the UV attenuation  $A(\lambda)$  estimated for the Lyman-break galaxies using the ‘starburst’ reddening curve and  $E(B-V)=0.15$  and, for comparison, the effective UV attenuation predicted by Model 3 at  $z=3$ . The two curves have a similar shape and the difference between the two attenuations is less than 13% over the entire wavelength range 1200-3000 Å. The implication is that, for all practical purposes, the two curves are equivalent.

The dependence of the dust temperature on  $\text{SFR}(z)$  (Equation 5) causes the dust to be hotter in high-redshift galaxies than in low- $z$  galaxies for Models 3 and 4 (e.g., Figure 9); however, the functional dependence is very weak, as it goes as a power  $1/(4+\epsilon)$ , so that the hottest galaxies have dust temperature between 35 and 40 K in all models. This is the typical dust temperature of local moderate starburst galaxies, like e.g. NGC7673 (Calzetti et al. 1995, Helou 1986). This clumpy irregular has a star formation rate of  $\sim 4 M_{\odot} \text{ yr}^{-1}$  within its central  $\sim 2$  kpc (Calzetti 1997b). For comparison, Lyman-break galaxies at  $z=3$  have an average observed  $\text{SFR}(1,500 \text{ \AA}) = 5 M_{\odot} \text{ yr}^{-1}$  within their half-light radii (Steidel et al. 1996), which corresponds to an attenuation-corrected  $\text{SFR}(1,500 \text{ \AA}) = 28 M_{\odot} \text{ yr}^{-1}$  for Model 3, or a star formation density of  $1 M_{\odot} \text{ yr}^{-1} \text{ kpc}^{-2}$ , similar to that found in NGC7673.

The measured metallicities of DLAs are  $\sim 1/15 Z_{\odot}$  in the redshift range  $2 < z < 3$  (Pettini et al.

1997b) and  $\sim 1/5$ – $1/10 Z_{\odot}$  at  $0.5 < z < 1$  (Boissè et al. 1998, Pettini et al. 1998b). As pointed out by Boissè et al., the measurements at  $z \sim 1$  could be a lower limit to the actual abundances of DLAs at those redshifts because dust obscuration will bias observations preferentially towards metal-poor systems. Assuming that the gas abundances in DLAs are representative of galaxies (see, however, Vladilo 1998 and Pettini et al. 1998b), Models 2, 3, 4 and 5 predict that the metallicity of the gas is  $\sim 1/40$ ,  $1/10$ ,  $1/6$ ,  $1/60 Z_{\odot}$ , respectively, in the redshift range  $2 < z < 3$  and  $\sim 0.3$ ,  $0.4$ ,  $0.6$ ,  $0.25 Z_{\odot}$ , respectively, at  $0.5 < z < 1$ . Among the four solutions, Model 3 gives the closest metallicity values to the observational data at high redshift. However, metal enrichment depends on the highly uncertain value of the effective yield  $\alpha_Z$ , which, in turn, depends on the stellar IMF (see discussion in Pagel 1987, 1998, Kauffmann & Charlot 1998). Thus the underabundance of Model 2 at high redshift may simply be a consequence of the uncertainty in the metal yield. The gas column densities at  $z=3$  implied by our solutions 2, 3, and 4 are in the range  $N(\text{H})=(5.4\text{--}12)\times 10^{21} \text{ cm}^{-2}$ , with the lowest value corresponding to Model 4 and the highest to Model 3. This range is comparable to the observed one,  $N_{*}(\text{HI})=(2\text{--}10)\times 10^{21} \text{ cm}^{-2}$  (Storrie-Lombardi, McMahon & Irwin 1996), once we take into account that our model gives the total column density in gas, while observational measurements of HI do not include molecular hydrogen. The  $z=3$  gas column density of Model 5 is  $N(\text{H})=3.5\times 10^{22} \text{ cm}^{-2}$ , much higher than what measured; this large value is a consequence of the large gas outflows required in Model 5 to constrain the final gas metallicity to  $Z_{\odot}$ . Gas inflows/outflows imply  $\Omega_{gas}(z=3)\sim 0.0035\text{--}0.008$  in Models 4 and 3, respectively. The gas density inferred from DLAs at the same redshift is  $\Omega_{gas}(z=3)\sim 0.0055$ , after correction for some reddening and for 20% gas fraction not in DLAs (Storrie-Lombardi et al. 1996). The measured value is a factor 1.5 higher/lower than predicted by our models. Allowances for uncertainties and/or incompleteness in the observations may in principle reduce some of the discrepancy. Another way to circumvent this difficulty is to allow in the models contemporary presence of inflows of metal-free gas in conjunction with outflows of metal-enriched gas. The outflows of Model 3 pollute the IGM with metals to the modest value of  $Z_{IGM}=0.05\text{--}0.07 Z_{\odot}$ , while Model 5 gives  $Z_{IGM}=0.08\text{--}0.11 Z_{\odot}$ , in the redshift range  $0.5 \leq z \leq 0$ . These values are a factor  $\sim 3\text{--}4$  smaller than what found in the intracluster medium (e.g., Mushotzky & Loewenstein 1997, Renzini 1997), but are comparable with observations of the Ly $\alpha$  Forest at  $z \sim 0.5$  (Barlow & Tytler 1998). Again,  $Z_{IGM}$  depends on the highly uncertain value of  $\alpha_Z$  (see below).

The shape of  $\text{SFR}_{int}$  of Model 3 resembles the ‘monolithic collapse’ formation model for stellar populations. About 20% of the total mass in stars today is produced at  $z > 3$  (within 2 Gy from the beginning of the Universe). If  $\sim 60\%$  of the local stellar mass is in old spheroids (Persic & Salucci 1992, Schechter & Dressler 1987), then 33% of the stars which are today in spheroids were formed at  $z > 3$ . These values agree with Renzini (1998), who argues on the basis of the intracluster medium metallicity that about 30% of all stars were produced at  $z > 3$ .

The functional shape of Model 3 is different from what found for, e.g., radio-loud (flat-spectrum) quasars (Shaver et al. 1996, 1998, Hook et al. 1998). Radio observations of these objects indicate a peak in space density around  $z=2.5$ ; the decrease in density beyond  $z=2.5$

has been suggested to be a real evolutionary effect (rather than dust obscuration, as suggested by Webster et al. 1995). The evolution of the space density of quasars resembles our Model 5. Shaver et al. have likened the evolution of the radio-loud quasars’ space density to the galaxy star formation history. However, such connection is not straightforward, as we don’t know, for instance, the details of the process which switches on a quasar, nor have we unraveled the relation between AGN activity and galaxy evolution. It is not clear yet that radio-selected samples are representative of the entire QSO population; thus, the possibility that dust obscuration is responsible for the high- $z$  decrease in the space density of optically-selected QSOs is not excluded yet.

## 4.2. The Impact of Parameter Choices

Using Model 3 as a baseline, we modify one by one some of the input parameters in the model, to assess their impact on the results.

### 4.2.1. *The Evolution of the Dust/Metal Ratio*

Our model uses the observational results of Pettini et al. (1997a) to infer the evolution of the dust/metals ratio with metallicity. If the dust/metals ratio instead depends only on the physics of the dust (e.g, the results of Vladilo 1998), and is constant and equal to the Milky Way value, the consequences for our model are pretty straightforward: low-metallicity systems will be more dusty. In particular, the predicted emergent-to-total light ratios decreases at all redshifts by  $\sim 60\text{--}70\%$ . Thus, the effect of an evolving dust/metals ratio is dramatic in low-metallicity objects.

### 4.2.2. *The Galaxy Spectral Energy Distribution*

Changing the input galaxy SED from a 1 Gyr constant star formation model to a 5 Gyr constant star formation model increases the fraction of optical-NIR bright stars relative to the UV. The CIB is the only output which uses the galaxy SED in our model, and, therefore, is the only quantity potentially affected. As mentioned in section 2.1.6, the bulk of the contribution to the galaxy FIR emission come from the UV stellar light reprocessed by dust; the contribution of the optical-IR stellar radiation is small in comparison. Indeed, when the CIB is computed from Model 3 using a constant star formation galaxy SED 5 Gyr old, instead of 1 Gyr old, the difference between the results is minimal: the intensity at  $\lambda < 300 \mu\text{m}$  is increased by 10–15%, while it is practically unchanged at longer wavelengths.

### 4.2.3. *The Dust Model*

The three basic assumptions on the dust model we have implemented are: the dust is homogeneously mixed with the stars with a wavelength-dependent scale height; the dust temperature depends on the surface density of the star formation rate (Equation 5) ; the value of the emissivity is  $\epsilon=2$ . These assumption are relaxed in turn in this section.

The homogeneous mixture of dust and stars appears to be a good representation of local galaxies (Xu & Buat 1995, Wang & Heckman 1996). However, high redshift galaxies may obey other geometrical descriptions; for instance the recently formed stars may be surrounded by, rather than mixed with, dust. This case has been implemented above in Model 5. Here, in order to bracket a range of situations, we consider two different geometries: 1. the dust surrounding the stellar population is in a uniform shell; 2. the dust surrounding the stellar population is distributed in clumps with a covering factor  $\sim 50\%$ . The results are shown in Figure 20. The UV opacities are overpredicted by the model of uniform dust (u) and underpredicted by the clumpy dust (c). In this sense, the two models bracket a range of dust geometries for galaxies, especially for the high redshift ones. It should be noted that the mixed geometry adopted throughout this paper produces opacities which are roughly the ‘middle point’ between the two geometries discussed in this section.

Observations suggest that the ‘average’ temperature of the dust in a galaxy is correlated with the density of the star formation activity (Lehnert & Heckman 1996). This behavior is reproduced in our model via Equation 5. The correlation is relaxed here to investigate its impact on the results. Figure 21 shows the case in which we adopt a dust temperature  $T=21$  K at all redshifts and independent of the star formation activity. A ‘cool’ FIR emission from high redshift galaxies in Model 3 implies too much flux in the CIB at long wavelengths ( $\lambda > 250 \mu\text{m}$ ) and too little flux at short wavelengths. This is understandable as the high redshift galaxies contribute to the longest wavelength part of the CIB.

Finally, we change the dust emissivity from  $\epsilon=2$  to  $\epsilon=1$ . These two values bracket the range observed in Galactic dust; the exact value of the dust emissivity is still unknown, although some authors favor values around  $\epsilon=(1.5,2.0)$  at long wavelengths (e.g., Désert et al. 1990). Figure 22 shows the effect of changing the value of the dust emissivity. The smaller value of the emissivity index implies that galaxies emit more flux at longer wavelengths. As a consequence, the predicted CIB has more power at  $\lambda \geq 250 \mu\text{m}$  relative to the  $\epsilon=2$  case, but fails to reproduce the intensity at  $\lambda < 200 \mu\text{m}$ . As discussed earlier, the FIR energy distribution of galaxies is more complex than the single temperature blackbody adopted here. Thus, the effect on the CIB of changing the dust emissivity index should be regarded only as indicative.

#### 4.2.4. The Metal Yield

The metal yields adopted throughout the paper are close to the median value observed in our Galaxy (Pagel 1987), although higher values cannot be excluded. The impact of higher  $\alpha_Z$  values on our results are straightforward: higher yields mean larger mass in metals. We have seen in Section 3 that changing the true yield  $\alpha_Z$  from 0.7 to 1.0 generally increases the UV opacities. If the final metallicity is constrained to  $Z_\odot$ , outflows must be present, implying that a larger initial galaxy mass is needed to outflow the larger mass in metals. Larger initial galaxy masses imply larger opacities at all redshifts. In numbers, by changing  $\alpha_Z$  from 0.7 to 1.0, the absolute variation of 1500 Å emergent-to-total UV light is  $\delta=(-0.08, -0.10)$  and the absolute variation of 2800 Å emergent-to-total UV light is  $\delta=-0.07$ , implying that the UV opacities are on average 40–50% higher.

### 5. Summary and Conclusions

We have built a model for the cosmic evolution of the dust opacity in galaxies in order to reconstruct the *intrinsic* SFR history of the Universe, free from the effects of dust obscuration. The model uses two basic constraints: the observed SFR density as a function of redshift, derived from UV observations of galaxies (Lilly et al. 1996, Madau et al. 1996, Connolly et al. 1997), and the Cosmic Infrared Background observed by COBE (Hauser et al. 1998, Fixsen et al. 1998). Additional constraints are provided by  $H\alpha$ , FIR and radio surveys of the local Universe and by the properties of the Lyman-break galaxies (e.g., Steidel et al. 1996, Giavalisco et al. 1996) and of the DLAs (e.g., Pettini et al. 1997a, 1998b) at high redshift.

The model converges to multiple solutions for the intrinsic SFR density (Figure 3) and the available observational constraints are still uncertain enough that no secure choice can be made for any of the solutions. The solutions can be separated into two main classes. The first class is represented by our Model 2, for which the intrinsic SFR has basically the same shape as the observed, UV-derived SFR, with a peak at  $z \simeq 1.2$ ; this solution corresponds to modest dust attenuations ( $2\times$ ) of the UV emission from galaxies at high redshift, but larger attenuations ( $\sim 4\times$ ) at  $z \leq 1$ . According to this model, about 3/4 of the UV emission from galaxies is hidden by dust in the low- $z$  Universe, while this fraction decreases to about 1/2 at  $z > 1.2$ . The intrinsic SFR density of Model 2 has the same intensity at  $z \sim 3$  and  $z \sim 0.3$ . The second class of solutions is represented by Model 3, for which the intrinsic SFR density is constant at high redshift and declines at  $z < 1.2$  with the same trend of the observed SFR density. Model 3 corresponds to relatively large dust attenuations of the UV emission from galaxies at high redshift ( $\sim 5\text{--}6\times$  at  $z \sim 3$ ) and smaller attenuations ( $\sim 3\times$ ) at  $z \leq 1$ . In other words, according to Model 3 local galaxies have on average enough dust opacity to ‘hide’ about 2/3 of the UV emission, while only  $\sim 1/5$  of the star formation emerges at UV wavelengths from  $z \sim 3$  galaxies. The two classes are mainly differentiated by the behavior of the intrinsic SFR at  $z > 1$ , in one case declining as the redshift



increases (Model 2), and in the other case constant with redshift (Model 3). Because of its shape, the solution Model 3 resembles the ‘monolithic collapse’ case for galaxy formation, and currently this solution satisfies the available observational constraints better than Model 2.

The various  $\text{SFR}_{int}$  we derive imply rather different distributions of the flux contribution to the CIB as a function of redshift. Model 3 predicts that most of the CIB flux at  $850\ \mu\text{m}$  originates at redshift greater than  $z\sim 2$ , while Model 2 predicts equal flux contributions from all galaxies at  $z>1$ . SCUBA observations should therefore be able to discriminate between the two models, once better redshift placements for the detected sources are secured.

It is worth noting that the input assumptions we have used to derive the self-consistent solutions tend to minimize the amount of dust produced (small metal yield, evolving dust/metal ratio) and its obscuring effects (mixed dust/star geometry). We have seen in section 4.2.5 that a 25% larger value for the metal yield immediately boosts up all UV opacities by  $\sim 50\%$ . Thus, under certain conditions galaxies may be even more opaque than what we have modelled.

Modelling the evolution of galaxies and their properties suffers from a number of uncertainties and unknowns about the physics of galaxy and star formation. Many of these have been detailed in Sections 2 and 4.2. The stellar IMF brings a factor  $\sim 2$  uncertainty in the derivation of the global SFR, because the low mass slope and cut-off mass are not measured with sufficient accuracy. Most likely, the uncertainty is in the direction of overestimating SFRs from the measurements of massive stars emission. Another question mark is whether the IMF has been constant with time or has changed as the physical conditions in galaxies (energy, metal, dust contents) changed. Linked to the IMF is the problem of the effective yield  $\alpha_Z$  (briefly discussed in section 4.2.5), which drives the metal and dust production and which even in our Galaxy is still uncertain by at least a factor 2 (Pagel 1987, 1998). Finally, uncertainties in the baryonic mass fraction in galaxies introduce another  $\sim 50\%$  uncertainty in models.

In conclusion, simple models of galaxy evolution indicate that star formation induces non negligible dust opacities at all redshifts ( $A_{1500} \sim 0.8\text{--}2$  at  $z>1$  and  $A_{2800} \sim 1.2\text{--}1.5$  at  $z\leq 1$ ). These opacities should be taken into account when reconstructing the global star formation history of the Universe from dust-sensitive observables. We emphasize that the attenuations derived here are perfectly adequate to reproduce the intensity and the spectral energy distribution of the CIB, arguing against the necessity of larger dust opacities in galaxies.

The idea for this paper was born during the Aspen Winter Workshop on ‘‘Universal Star Formation’’ (January 1998), from discussions with Rosemary Wyse, Mauro Giavalisco and Alvio Renzini. D.C. acknowledges the hospitality of the Observatories of the Carnegie Institution of Washington, where part of this work was developed. The authors also thank Mark Dickinson for elucidating the properties of the high redshift galaxies.

## REFERENCES

- Armus, L., Soifer, B.T., Murphy, T.W., Neugebauer, G., Evans, A.S., & Matthews, K. 1998a, *ApJ*, 495, 276
- Armus, L., Matthews, K., Neugebauer, G., & Soifer, B.T. 1998b, *ApJ*, in press (Letters)
- Aragon-Salamanca, A., Baugh, C.M., & Kauffmann, G. 1998, *MNRAS*, 297, 427
- Barger, A.J., Cowie, L.L., Sanders, D.B., Fulton, E., Taniguchi, Y., Sato, Y., Kawara, K. & Okuda, H. 1998, *Nature*, embargoed (astro-ph/9806317)
- Barlow, T.A., & Tytler, D. 1998, *AJ*, 115, 1725
- Baugh, C.M., Cole, S., & Frenk, C.S. 1996, *MNRAS*, 283, 1361
- Berlind, A.A., Quillen, A.C., Pogge, R.W., & Sellgren, K. 1997, *AJ*, 114, 107
- Bohlin, R.C., Savage, B.D., & Drake, J.F. 1978, *ApJ*, 224, 132
- Boissé, P., Le Brun, V., Bergeron, J., & Deharveng, J.-M. 1998, *A&A*, 333, 841
- Bouchet, P., Lequeux, J., Maurice, E., Prevot, L., & Prevot-Burnichon, M.L. 1985, *A&A*, 149, 330
- Bruzual, G. A., & Charlot, S. 1996, private communication
- Buat, V., & Burgarella, D. 1998, *A&A*, in press
- Calzetti, D. 1997a, in *The Ultraviolet Universe at Low and High Redshift: Probing the Progress of Galaxy Evolution*, eds. W.H. Waller, M.N. Fanelli, J.E. Hollis & A.C. Danks, *AIP Conf. Proc.* 408 (Woodbury: AIP), 403
- Calzetti, D. 1997b, *AJ*, 113, 162
- Calzetti, D., Kinney, A.L., & Storchi-Bergmann, T. 1994, *ApJ*, 429, 582
- Calzetti, D., Bohlin, R.C., Kinney, A.L., Storchi-Bergmann, T., & Heckman, T.M. 1995, *ApJ*, 443, 136
- Cram, L.E. 1998, *ApJ*, in press (Letters)
- Connolly, A.J., Szalay, A.S., Dickinson, M., Subbarao, M.U., & Brunner, R.J. 1997, *ApJ*, 486, L11
- Cox, P., Krügel E., & Mezger P.G. 1986, *A&A*, 155, 380
- Dehnen, W., & Binney, J. 1998, *MNRAS*, 294, 429
- Désert, F.-X., Boulanger, F., & Puget, J.L. 1990, *A&A*, 237, 215
- Dey, A., SPinrad, H., & Dickinson, M. 1995, *ApJ*, 440, 515

- Dickinson, M. 1998, in *The Hubble Deep Field*, STScI May Symposium, eds. M. Livio, S.M. Fall, & P. Madau, (Cambridge: CUP), in press
- Downes, D., & Solomon, P.M. 1998, *ApJ*, in press
- Dwek, E. 1998, *ApJ*, 501, 643
- Eales, S., Lilly, S., Gear, W., Dunne, L., Bond, J.R., Hammer, F., Le Fèvre, O., & Crampton, D. 1998, *ApJ*, submitted (Letters)
- Edmunds, M.G., & Phillips, S. 1997, *MNRAS*, 733, 747
- Fitzpatrick, E.L. 1989, *AJ*, 92, 1068
- Fixsen, D.J., Dwek, E., Mather, J.C., Bennett, C.L., Shafer, R.A. 1998, *ApJ*, in press
- Fukugita, M., Hogan, C.J., & Peebles, P.J.E. 1998, *ApJ*, submitted
- Gallego, J., Zamorano, J., Aragon-Salamanca, A., & Rego, M. 1995, *ApJ*, 455, L1
- Giavalisco, M., Steidel, C.C., & Macchetto, F.M. 1996, *ApJ*, 470, 189
- Giavalisco, M., et al. 1998, in prep.
- Giovanelli, R., Haynes, M.P., Salzer, J.J., Wegner, G., Da Costa, L.N., & Freudling, W. 1995, *AJ* 110, 1059
- Gnedin, N. Yu., & Ostriker, J.P. 1992, *ApJ*, 400, 1
- Gonzalez, R.A., Allen, R.J., Dirsch, B., Ferguson, H.C., Calzetti, D., & Panagia N. 1998, *ApJ*, in press
- Gordon, K.D., Calzetti, D., & Witt, A.N. 1997, *ApJ*, 487, 625
- Gronwall, C., 1998, in *Dwarf Galaxies and Cosmology, the XXXIIIrd Recontres de Moriond*, eds. T.X. Thuan, C. Balkowski, V. Cayatte & J. Tran Thanh Van (Gif-sur-Yvette: Editions Frontières), in press
- Hammer, F. & Flores, H. 1998, in *Dwarf Galaxies and Cosmology, the XXXIIIrd Recontres de Moriond*, eds. T.X. Thuan, C. Balkowski, V. Cayatte & J. Tran Thanh Van (Gif-sur-Yvette: Editions Frontières), in press (astroph/9806184)
- Hauser, M.G., Arendt, R.G., Kelsall, T., Dwek, E., Odegard, N., Weiland, J.L., Freudenreich, H.T., Reach, W.T., Silverberg, R.F., Moseley, S.H., Pei, Y.C., Lubin, P., Mather, J.C., Shafer, R.A., Smoot, G.F., Weiss, R., Wilkison, D.T., & Wright, E.L. 1998, *ApJ*, accepted for publ.
- Helou, G., 1986, *ApJ*, 311, L33

- Hook, I.M., Shaver, P.A., & McMahon, R.G. 1998, in *The Young Universe: Galaxy Formation and Evolution at Intermediate and High Redshift*, eds. S. D’Odorico, A. Fontana, & E. Giallongo, ASP Conf. Series, in press
- Hughes, D., Serjeant, S., Dunlop, J., Rowan-Robinson, M., Blain, A., Mann, R.G., Ivison, R., Peacock, J., Efstathiou, A., Gear, W., Oliver, S., Lawrence, A., Longair, M., Goldschmidt, P., & Jenness, T. 1998, *Nature*, 394, 241
- Hunter, D. A., O’Neil, Jr., E. J., Lynds, R., Shaya, E. J., et al. 1996, *ApJ*, 459, L27
- Hunter, D. A., Light, R. M., Holtzman, J. A., Lynds, R., et al. 1997, *ApJ*, 478, 124
- Ivison, R.J., Smail, I., Le Borgne, J.-F., Blain, A.W., Kneib, J.-P., Bezecourt, J., Kerr, T.H., & Davies, J.K. 1998, *MNRAS*, 298, 583
- Jones, A.P., Tielens, A.G.G.M., Hollenbach, D.J., & McKee, C.F. 1994, *ApJ*, 433, 797
- Kauffman, G. 1996, *MNRAS*, 281, 487
- Kauffmann, G., & Charlot, S. 1998, *MNRAS*, 294, 705
- Kauffmann, G., Charlot, S., & White, S.D.M. 1996, *MNRAS*, 283, L117
- Kennicutt, R.C., 1998, *ApJ*, 498, 541
- Kennicutt, R.C., Tamblyn, P., & Congdon, C.E. 1994, *ApJ*, 435, 22
- Kroupa, P. 1995, *MNRAS* 277, 1491
- Krugel, E., Siebenmorgen, R., Zota, V., & Chini, R. 1998, *A&A*, 331, L9
- Kunth, D., Matteucci, F., & Marconi, G. 1995, *A&A*, 297, 634
- Kylafis, N.D., & Bahcall. J.N. 1987, *ApJ*, 317, 637
- Larson, R.B. 1998, *MNRAS*, in press (astro-ph/9808145)
- Lehnert, M.D., & Heckman, T.M. 1996, *ApJ*, 472, 546
- Leitherer, C., & Heckman, T.M. 1995, *ApJS*, 96, 9
- Lilly, S., Eales, S.A., Gear, W.K., Bond, J.R., Dunne, L., Hammer, F., Le Fèvre, O., & Crampton, D. 1998, in *NGST: Science and Technological Challenges*, to be published by the European Space Agency
- Lilly, S.J., Le Fèvre, O., Hammer, F. & Crampton, D. 1996, *ApJ*, 460, L1
- Lonsdale-Persson, C.J., & Helou, G. 1987, *ApJ*, 314, 513

- Lowenthal, J., Koo, D., Guzman, R., Gallego, J., Phillips, A.C., Faber, S.M., Vogt, N.P., Illingworth, G.D., & Gronwall, C. 1997, *ApJ*, 481, 673
- Madau, P., Ferguson, H.C., Dickinson, M.E., Giavalisco, M., Steidel, C.C., & Fruchter, A. 1996, *MNRAS*, 283, 1388
- Madau, P., Pozzetti, L., & Dickinson, M. 1998, *ApJ*, 498, 106
- Marzke, R.O., Huchra, J.P., & Geller, M.J. 1994, *ApJ*, 428, 43
- Massey, P., Lang, C. C., DeGioia-Eastwood, K., & Garmany, C. D. 1995, *ApJ*, 438, 188
- Meurer, G. R., Heckman, T.M., Lehnert, M.D., Leitherer, C., & Lowenthal, J. 1997, *AJ*, 114, 54
- Meurer, G. R., Heckman, T. M., & Calzetti, D. 1998, in preparation
- Moriondo, G., Giovanelli, R., & Haynes, M.P. 1998, *A&A*, in press.
- Mushotzky, R.F., & Loewenstein, M. 1997, *ApJ*, 481, L63
- Omont, A., McMahon, R.G., Cox, P., Kreysa, E., Bergeron, J., Pajot, F., & Storrie-Lombardi, L.J. 1996, *A&A*, 315, 1
- Ortolani, S., Renzini, A., Gilmozzi, R., Marconi, G., Barbuy, B., Bica, E., & Rich, M.R. 1995, *Nature*, 377, 701
- Pagel, B.E.J. 1987, in *The Galaxy*, G. Gilmore & B. Carswell eds. (Dordrecht: Reidel), 341
- Pagel, B.E.J. 1998, in *Dwarf Galaxies and Cosmology, the XXXIIIrd Recontres de Moriond*, eds. T.X. Thuan, C. Balkowski, V. Cayatte & J. Tran Thanh Van (Gif-sur-Yvette: Editions Frontières), in press
- Pei, Y.C., & Fall, S.M. 1995, *ApJ*, 454, 69
- Pettini, M., Ellison, S.L., Steidel, C.C., & Bowen, D.V. 1998b, *ApJ*, in press
- Pettini, M., Kellogg, M., Steidel, C.C., Dickinson, M., Adelberger, K.L., & Giavalisco, M. 1998a, *ApJ*, in press
- Pettini, M., King, D.L., Smith, L.J., & Hunstead, R.W. 1997a, *ApJ*, 478, 536
- Pettini, M., Smith, L.J., King, D.L., & Hunstead, R.W. 1997b, *ApJ*, 486, 665
- Persic, M., & Salucci, P. 1992, *MNRAS*, 258, 14P
- Phillips, A.C., Bershad, M.A., Forbes, D.A., Koo, D.C., Illingworth, G.D., Reitzel, D.B., Griffith, R.E., & Windhorst, R.A. 1995, *ApJ*, 444, 21
- Renzini, A. 1997, *ApJ*, 488, 35

- Renzini, A. 1998, in *The Young Universe: Galaxy Formation and Evolution at Intermediate and High Redshift*, eds. S. D’Odorico, A. Fontana, & E. Giallongo, ASP Conf. Series, in press
- Rowan-Robinson, M., & Crawford, J. 1989, *MNRAS*, 238, 523
- Rowan-Robinson, M., et al. 1997, *MNRAS*, 289, 490
- Sawicki, M., & Yee, H. K. C. 1998, *AJ*, in press
- Scalo, J. M. 1998, in *Proc. 38th Herstmonceaux Conf. on the Stellar IMF*, ed. Gilmore, Parry, & Ryan, in press.
- Schramm, D.N., & Turner, M.S. 1998, *Rev. Mod. Phys.*, 70, 303
- Schechter, P.L., & Dressler, A. 1987, *AJ*, 94, 563
- Scoville, N.Z., Evans, A.S., Dinshaw, N., Thompspn, R., Rieke, M., Schneider, G., Low, F.J., Hines, D., Stobie, B., Becklin, E., & Hepps, H. 1998, *ApJ (Letters)*, in press
- Shaver, P.A., Hook, I.M., Jackson, C.A., Wall, J.V., Kellermann, K.I. 1998, in *Highly Redshifted Radio Lines*, eds. C. Carilli, S. Radford, K. Menten, & G. Langston (San Francisco: PASP), in press
- Shaver, P.A., Wall, J.V., Kellermann, K.I., Jackson, C.A., & Hawkins, M.R.S. 1996, *Nature*, 384, 439
- Sirianni, M., Nota, A., Leitherer, C., De Marchi, G., & Clampin, M. 1998, in prep.
- Smail, I., Ivison, R.J., & Blain, A.W. 1997, *ApJ*, 490, L5
- Soifer, B.T., & Neugebauer, G. 1991, *AJ*, 101, 354
- Steidel, C.C., Adelberger, K.L., Giavalisco, M., Dickinson, M., Pettini, M., & Kellogg, M. 1998, proceedings of the Royal Society Discussion Meeting, *Phil. Trans. R. Soc. Lond.*, in preparation
- Steidel, C.C., Giavalisco, M., Pettini, M., Dickinson, M., & Adelberger, K.L. 1996, *ApJ*, 462, L17
- Storrie-Lombardi, L.J., McMahon, R.G., & Irwin, M.J. 1996, *MNRAS*, 283, L79
- Tielens, A.G.G.M. 1990, in *Carbon in the Galaxy*, ed. J.C. Tarter, S. Chang, & D. De Frees (NASA CP 3061), 59
- Tosi, M. 1998, in *Dwarf Galaxies and Cosmology, the XXXIIIrd Recontres de Moriond*, eds. T.X. Thuan, C. Balkowski, V. Cayatte & J. Tran Thanh Van (Gif-sur-Yvette: Editions Frontières), in press
- Treyer, M.A., Ellis, R.S., Milliard, B., Donas, J., & Bridges, T.J. 1998, *MNRAS*, in press

- Trewhella, M. 1997, in *The Ultraviolet Universe at Low and High Redshift: Probing the Progress of Galaxy Evolution*, eds. W.H. Waller, M.N. Fanelli, J.E. Hollis & A.C. Danks, AIP Conf. Proc. 408 (Woodbury: AIP), 349
- Villumsen, J.V., & Strauss, M.A. 1987, *ApJ*, 322, 37
- Vladilo, G. 1998, *ApJ*, 493, 583
- Wang, B., & Heckman, T.M. 1996, *ApJ*, 457, 645
- Webster, R.L., Francis, P.J., Peterson, B.A., Drinkwater, M.J., & Masci, F.J. 1995, *Nature*, 375, 469
- White, S.D.M., & Frenk, C.S. 1991, *ApJ*, 379, 25
- White, R.E., Keel, W.C., & Conselice, C.J. 1996, pre-print (astro-ph/9604029)
- Williams, R.E., et al. 1996, *AJ*, 112, 1335
- Witt, A.N., & Gordon, K.D. 1996, *ApJ*, 463, 681
- Witt, A.N., Thronson, H.A., & Capuano, J.M. 1992, *ApJ*, 393, 611
- Worthey, G. 1994, *ApJS*, 95, 107
- Xu, C., & Buat, V. 1995, *A&A*, 293, L65
- Yamashita, K. 1992, in *Frontiers of X-ray Astronomy*, eds. Y. Tanaka & K. Koyama (Tokyo: Universal Academy Press), 475
- Young, J.S., Xie, S., Kenney, J.D.P., & Rice, W.L. 1989, *ApJS*, 70, 699.

TABLE 1  
CHARACTERISTICS OF THE MODELS

Model	Envir. <sup>a</sup>	$\alpha_Z$ <sup>b</sup>	$f_{mass}(z = \infty)$ <sup>c</sup>	$Z_{gas}(z=0)$ <sup>d</sup>	$N_H(z=0)$ <sup>e</sup>	dust/met <sup>f</sup>	$E(B-V)_p$ <sup>g</sup>	$f_{star}$ <sup>h</sup>	$\Sigma_{eff}/\Sigma_{inst}$ <sup>i</sup>
1	C	0.7	0.00	0.16	7.22E+21	Y	0.11(z=0.0)	0.20	N
2	C	0.7	0.00	0.76	3.01E+21	Y	0.36(z=0.0)	0.66	Y
3	O	0.7	0.41	1.00	1.18E+21	Y	0.32(z=1.8)	0.87	Y
4	I	0.7	0.48	1.00	1.71E+21	Y	0.31(z=0.4)	0.81	Y
5	O	1.0	0.76	1.00	0.54E+21	N	1.20(z=1.2)	0.94	Y

<sup>a</sup>Interaction of the galaxies with the environment: closed-box (C), outflows (O) or inflows (I).

<sup>b</sup>True metal yield (units of  $Z_{\odot}$ ).

<sup>c</sup>Fraction of the initial ( $z=\infty$ ) mass lost because of outflows or acquired because of inflows.

<sup>d</sup>Gas metallicity in the present-day galaxies, in units of  $Z_{\odot}$ .

<sup>e</sup>Average hydrogen column density in present-day galaxies.

<sup>f</sup>Dust/Metal ratio evolving (Y) or not evolving (N) with metallicity.

<sup>g</sup>Peak dust column density (and redshift of the peak).

<sup>h</sup>Fraction of the present-day galaxy mass which is locked in stars.

<sup>i</sup>Presence (Y) or absence (N) of an evolving surface mass density for the galaxies (Figure 1 and section 2.1.5).



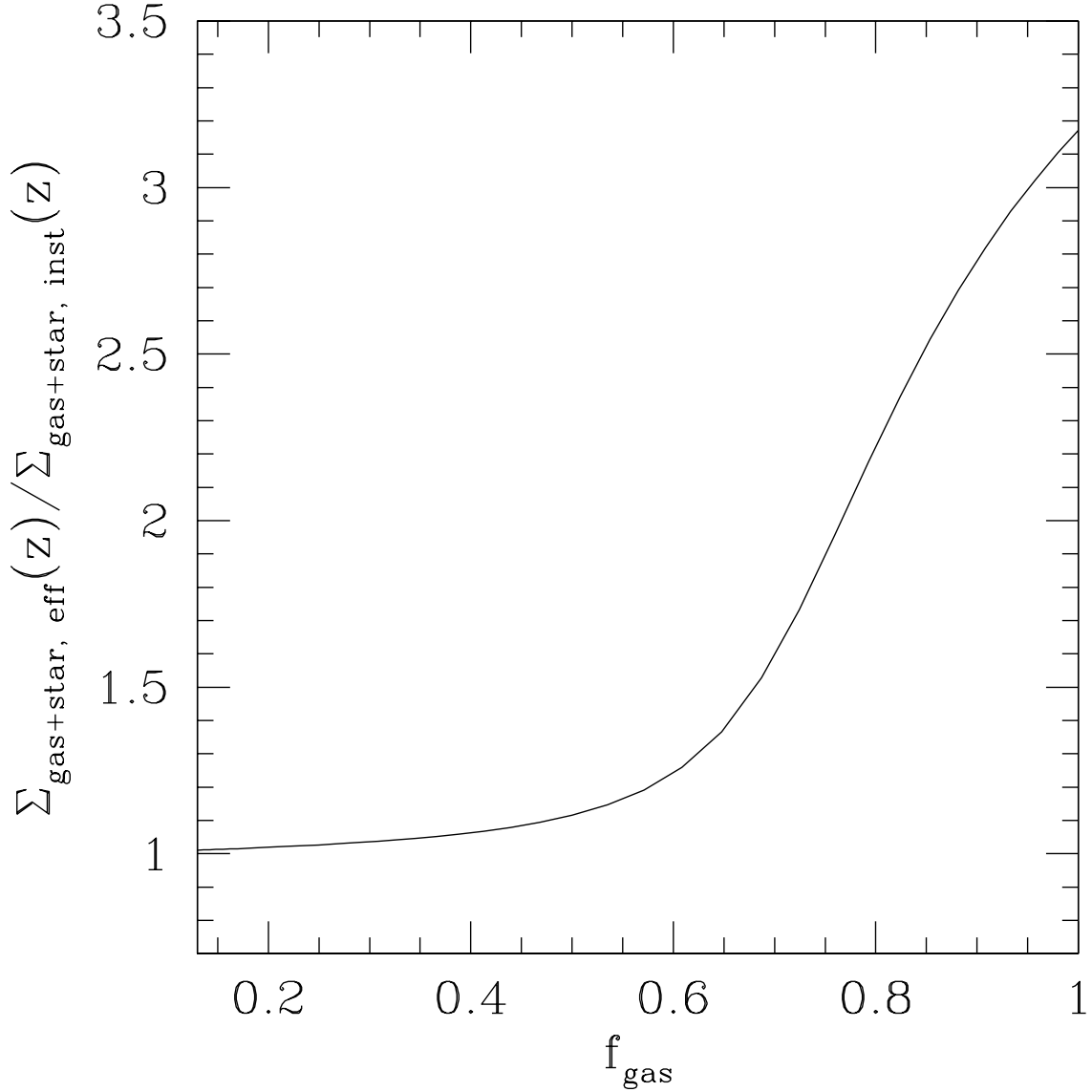


Fig. 1.— The ratio of the effective-to-instantaneous surface mass density  $\Sigma_{\text{gas+star, eff}}(z) / \Sigma_{\text{gas+star, inst}}(z)$ , as a function of the gas fraction in the galaxy.  $\Sigma_{\text{gas+star, inst}}(z)$  is the average surface mass density at redshift  $z$  from the outflow/closed-box/inflow models.  $\Sigma_{\text{gas+star, eff}}(z)$  is the effective surface mass density observed in high redshift galaxies, possibly due to concentrated star formation. The ratio  $\Sigma_{\text{gas+star, eff}}(z) / \Sigma_{\text{gas+star, inst}}(z)$  is used to model the effective dust column density and temperature in high redshift galaxies.

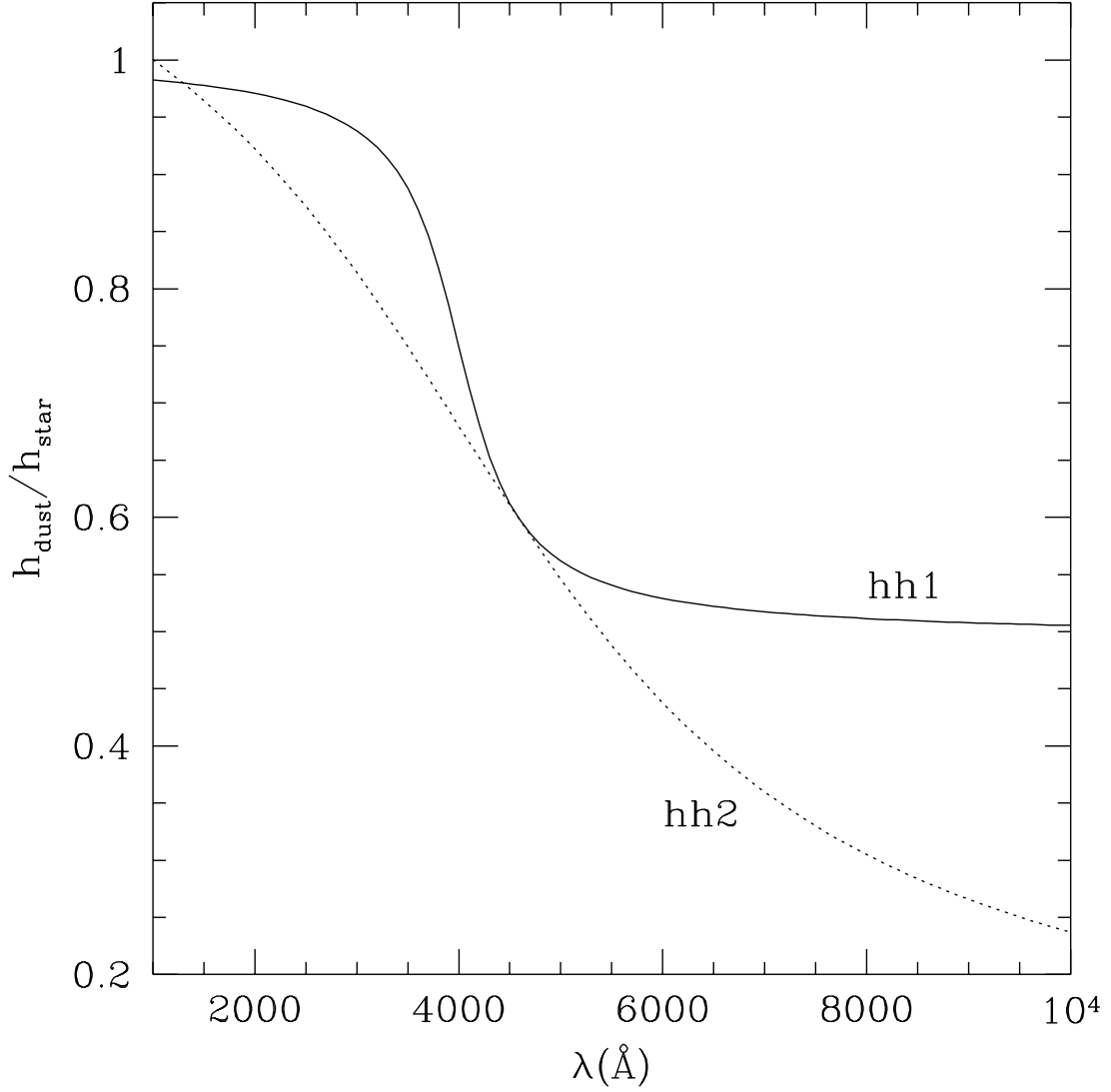


Fig. 2.— The two representations of the scaleheight ratio of dust to stars,  $h_{\text{dust}}/h_{\text{star}}$ , adopted throughout the paper are shown here as a function of wavelength. In the first representation, labelled ‘hh1’, the scaleheight ratio is  $\sim 1$  in the UV and is  $\sim 0.5$  at optical wavelengths, with a sharp change around  $4000 \text{ \AA}$ . The second representation, labelled ‘hh2’, accomodates a smoother change in the scaleheight ratio, from  $\sim 1$  at  $1000 \text{ \AA}$  to  $\sim 0.25$  at  $10000 \text{ \AA}$ .

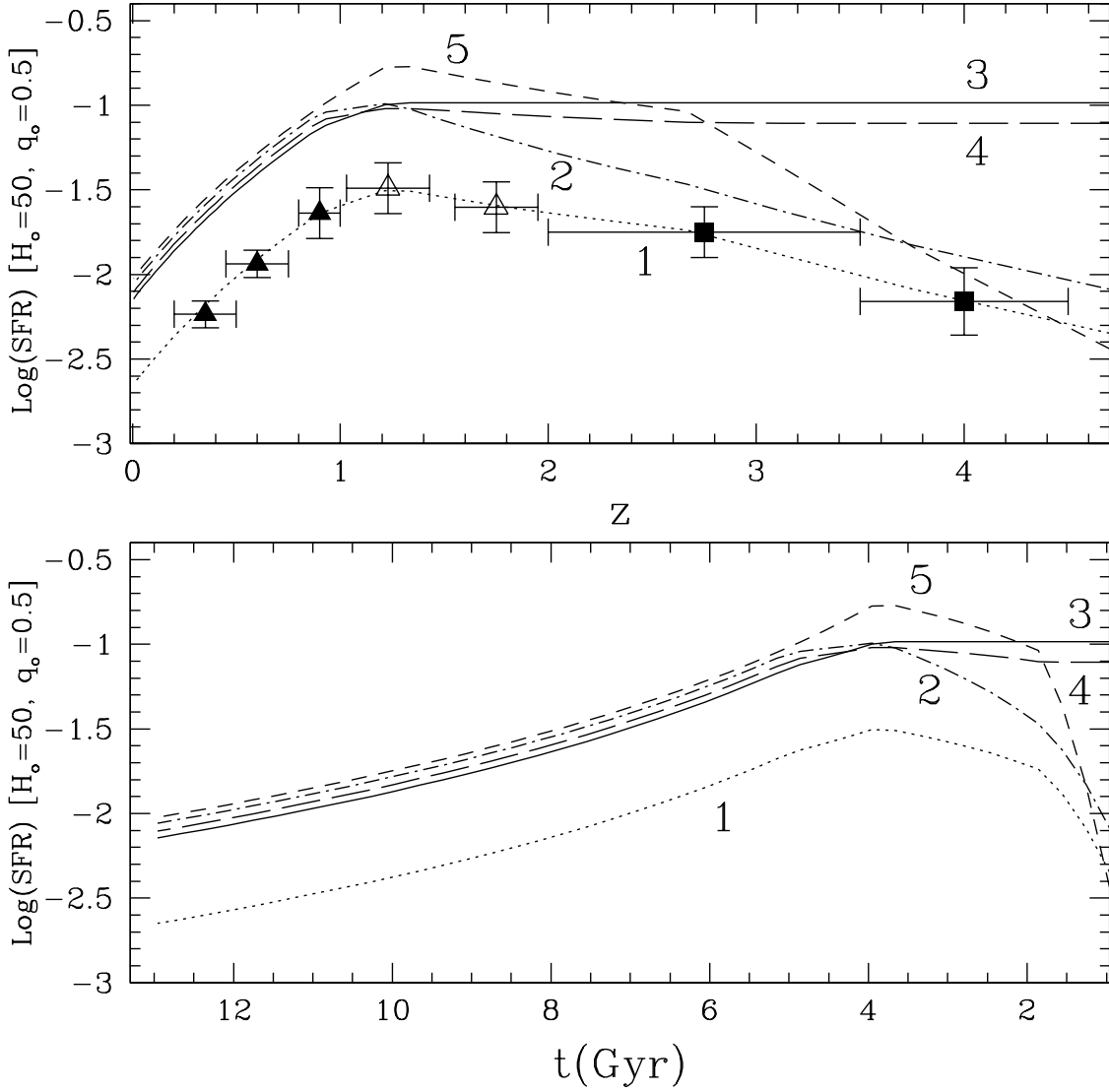


Fig. 3.— The observed and intrinsic star formation rate densities SFR, in units of  $M_{\odot} \text{ yr}^{-1} \text{ Mpc}^{-3}$ , are shown as a function of both redshift (top panel) and time (bottom panel). The observed SFR,  $\text{SFR}_{obs}$  is labelled as Model 1 (dotted line), and represents a smooth interpolation of the data points. The data are from the observed UV flux densities reported by Lilly et al. (1996, filled triangles) and Connolly et al. (1997, empty triangles) at  $2800 \text{ \AA}$ , and by Madau et al. (1998, filled squares) at  $1500 \text{ \AA}$ . The other four models are the intrinsic star formation rate densities,  $\text{SFR}_{int}$ , which are solutions of our iterative procedure; the solutions are labelled Model 2 through 5 and their main characteristics are listed in Table 1. Models 2 (dot-dashed line), 3 (continuous line), and 4 (long-dashed line) are solutions for closed-box, outflows and inflows galaxy models, respectively. Model 5 is obtained from extreme choices of some of the model’s parameters (see text). In all cases the low redshift  $\text{SFR}_{int}$  is similar in amplitude, while most of the difference occurs at  $z > 1$ , namely at ages of the Universe  $< 4 \text{ Gyr}$  ( $H_o = 50 \text{ km/s/Mpc}$  and  $q_o = 0.5$ ).

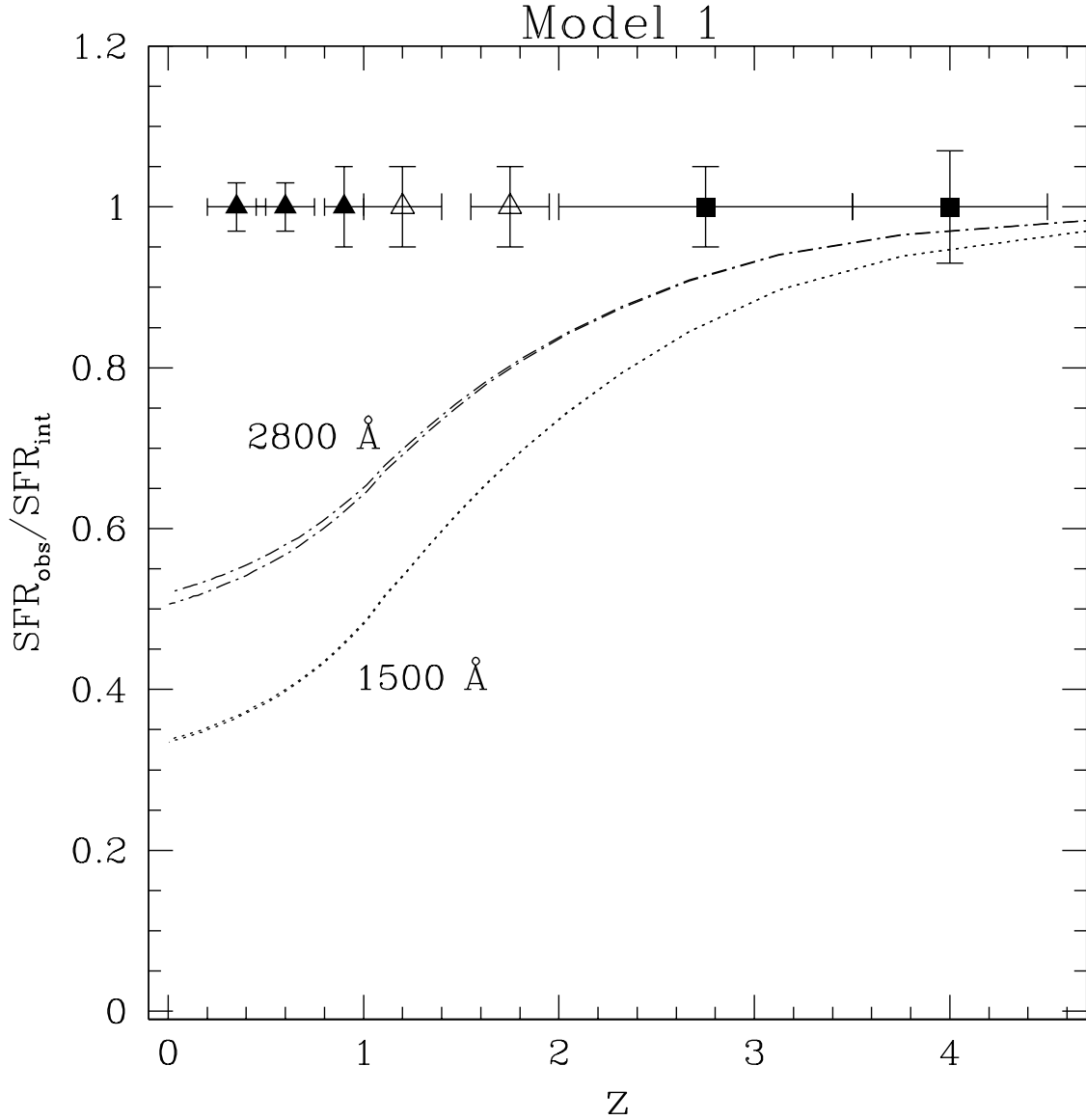


Fig. 4.— The ratio between the observed and intrinsic star formation rate density, SFR, is shown as a function of redshift. The data points (filled and empty triangles and filled squares) show the ratio  $\text{SFR}_{\text{obs}}/\text{SFR}_{\text{int}}$  using the  $\text{SFR}_{\text{obs}}$  of Figure 3. Here the ratio is unity because  $\text{SFR}_{\text{int}}=\text{SFR}_{\text{obs}}$  by construction in Model 1. The continuous lines are the emerging-to-total radiation predicted by the input star formation rate,  $\text{SFR}_{\text{int}}$ , at  $2800 \text{ \AA}$  (dash-dotted line) and  $1500 \text{ \AA}$  (dotted line), respectively. At each fixed wavelength, two lines are shown and correspond to the two adopted scaleheight ratios,  $h_{\text{dust}}/h_{\text{star}}$  (Figure 2): the lower values of the emerging-to-total radiation correspond to hh1, while the larger values correspond to hh2. For  $\text{SFR}_{\text{int}}$  to be a solution of the model, the  $\text{SFR}_{\text{obs}}/\text{SFR}_{\text{int}}$  points must lay on top of the opacity curve at the appropriate wavelength. It is clear that Model 1 is an unacceptable solution.

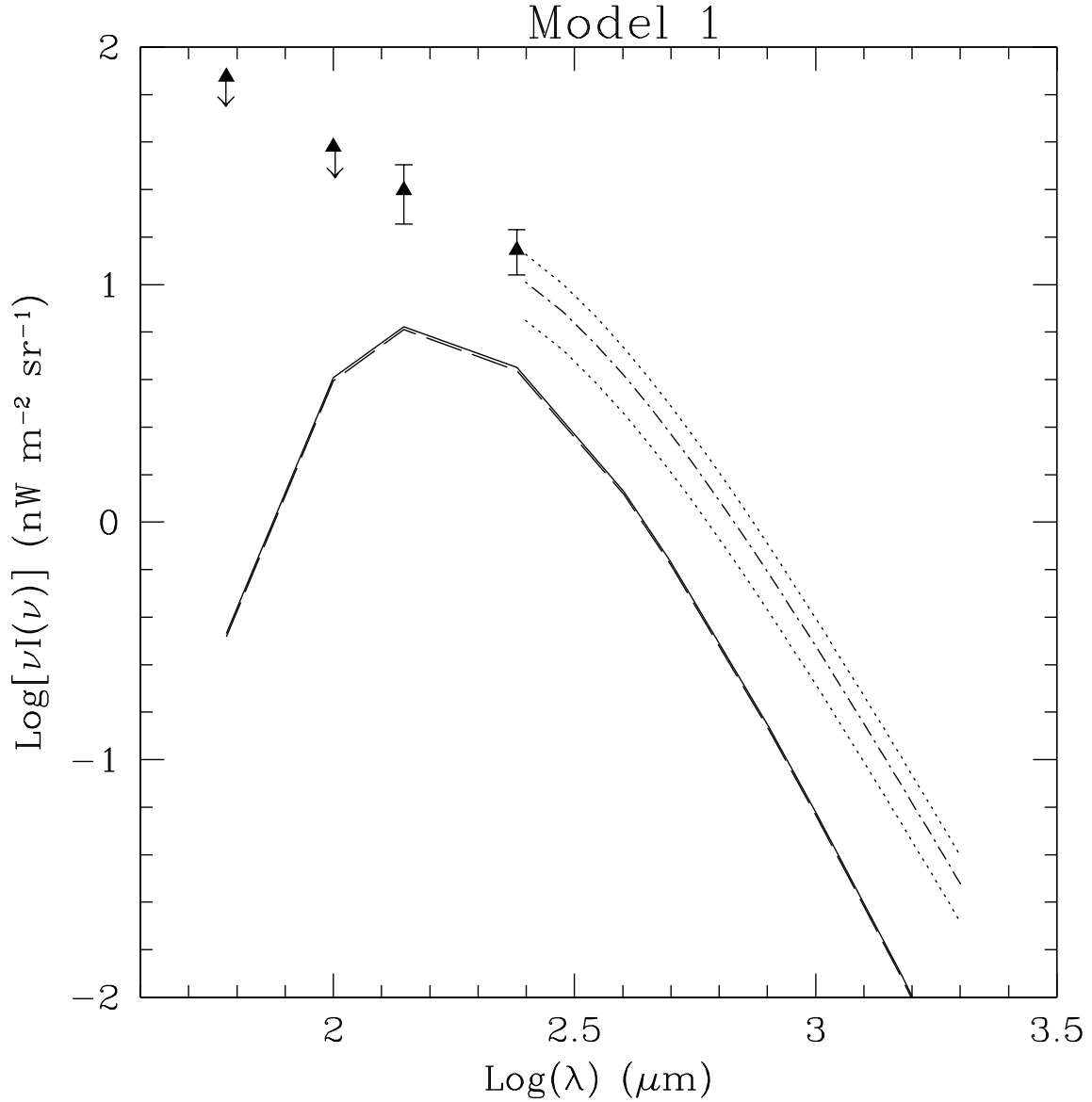


Fig. 5.— The FIR background predicted by Model 1 is compared with the data from COBE DIRBE and FIRAS. The continuous line is the model prediction for the dust/star scaleheight ratio  $hh_1$  and the long-dashed line is the model prediction for  $hh_2$  (see Figure 2). The DIRBE data are indicated as filled triangles with  $1\sigma$  error bars; the values at  $60\ \mu\text{m}$  and  $100\ \mu\text{m}$  are upper limits. The FIRAS values are reported as the best fit to the data given in Fixsen et al. (1998, dot-dashed line) together with the fiducial  $1\sigma$  error bar (dotted lines). Model 1 produces only  $\sim 25\%$  of the observed FIR flux, with no significant variation between the two dust/star scaleheight ratios.

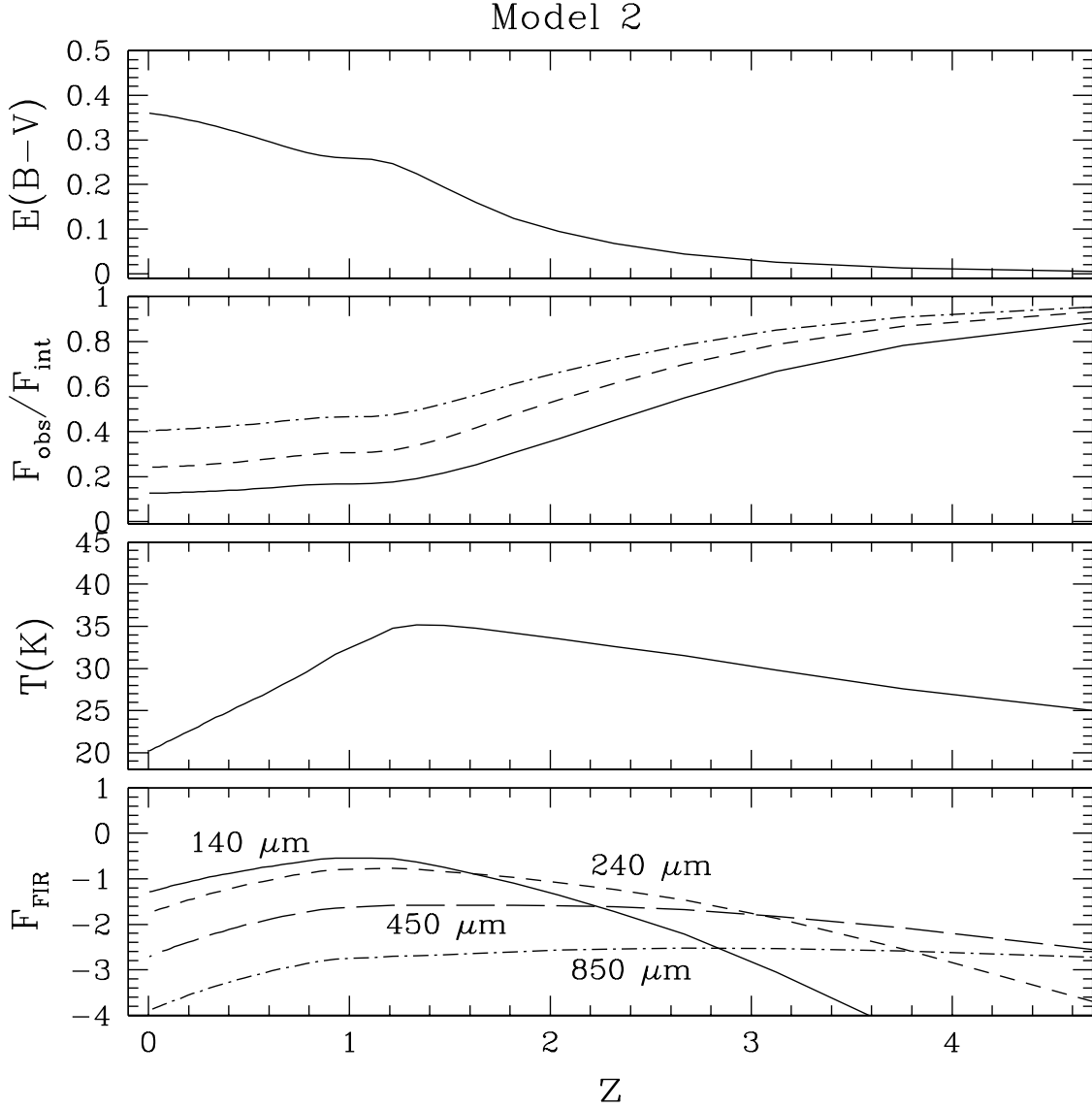


Fig. 6.— The evolution of the dust column density, the opacity and the FIR emission as a function of the redshift  $z$  for the  $\text{SFR}_{\text{int}}$  of Model 2 (cf. Figure 3). The first panel from the top shows the evolution of the dust column density  $E(B-V)$ . The second panel shows the ratio of emerging-to-total radiation for a few representative UV-B wavelengths in the galaxy’s restframe: 1500 Å (solid line), 2800 Å (dashed line), and 4400 Å (dot-short dash line). The third panel shows the evolution of the dust temperature in K. The fourth panel shows the contributing flux to the CIB, in arbitrary units, at selected wavelengths in the observer’s restframe, 140 μm, 240 μm, 450 μm and 850 μm. The dust/star scaleheight ratio adopted in this figure is hh1 (Figure 2).

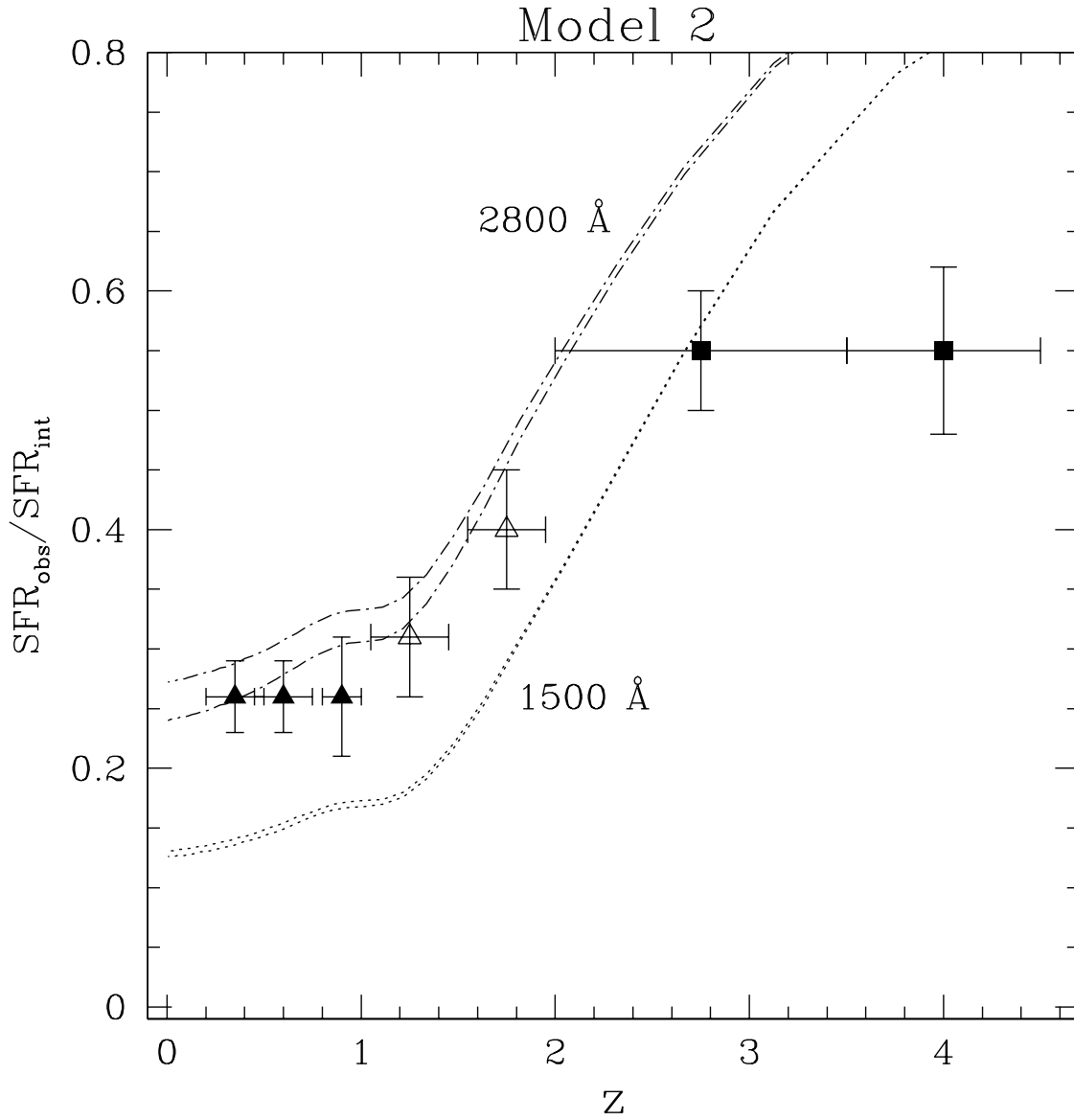


Fig. 7.— As Figure 4, for the  $SFR(z)$  of Model 2. The ratio  $SFR_{obs}/SFR_{int}$  at  $z < 2$ , which is equivalent to the emergent-to-total light at 2800 Å, overlaps with the predicted opacity curve at the same wavelength. The same happens for the  $SFR_{obs}/SFR_{int}$  point at  $z = 2.75$ , which is equivalent to the emergent-to-total light at 1500 Å. This figure shows that  $SFR_{int}(z)$  of Model 2 is a solution of our self-consistent procedure as the predicted UV opacities account for  $SFR_{obs}(z)$ .

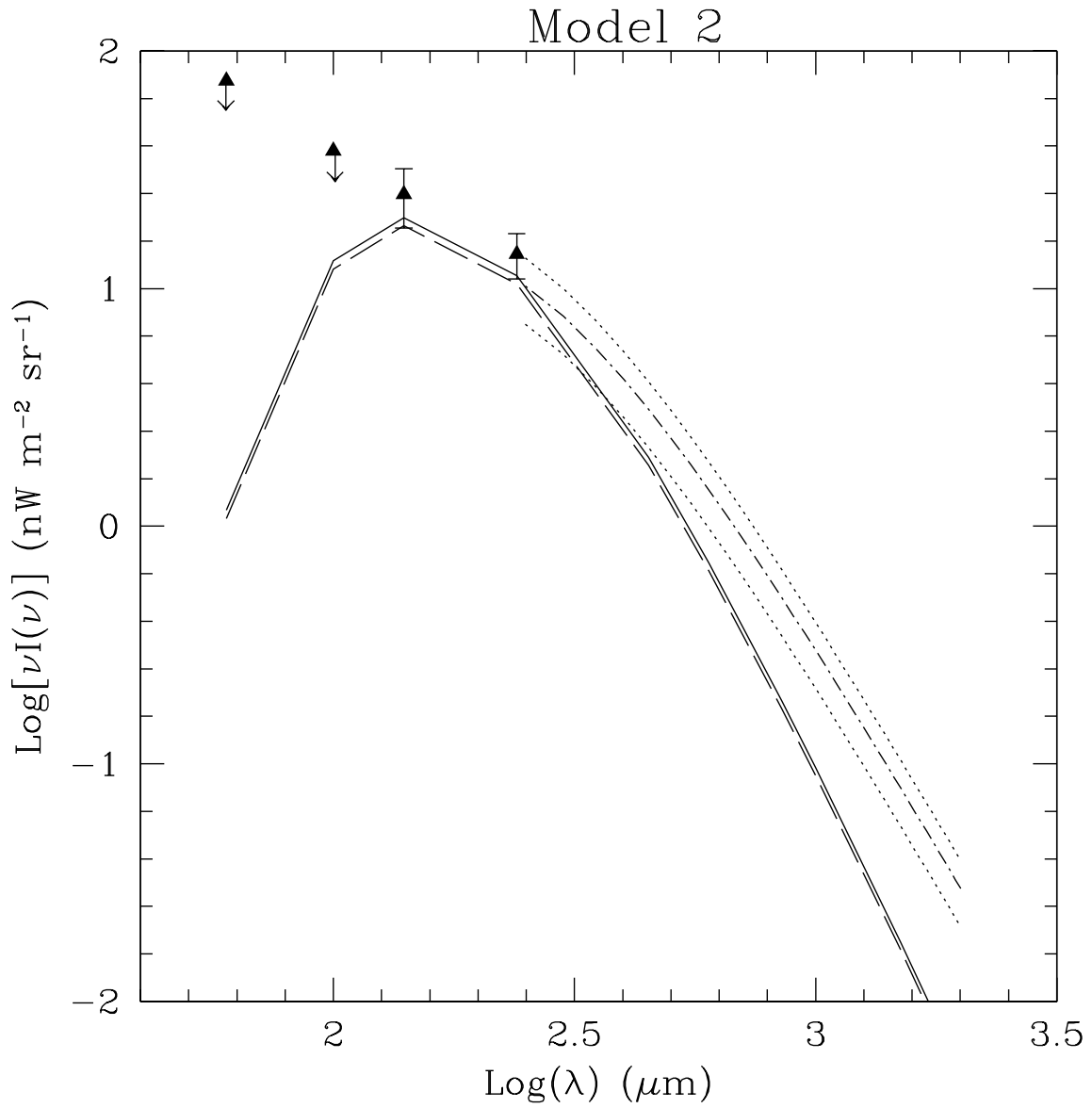


Fig. 8.— The FIR background predicted by the  $\text{SFR}_{int}$  of Model 2 is compared with the data from COBE DIRBE and FIRAS. The symbols and lines are as in Figure 5.



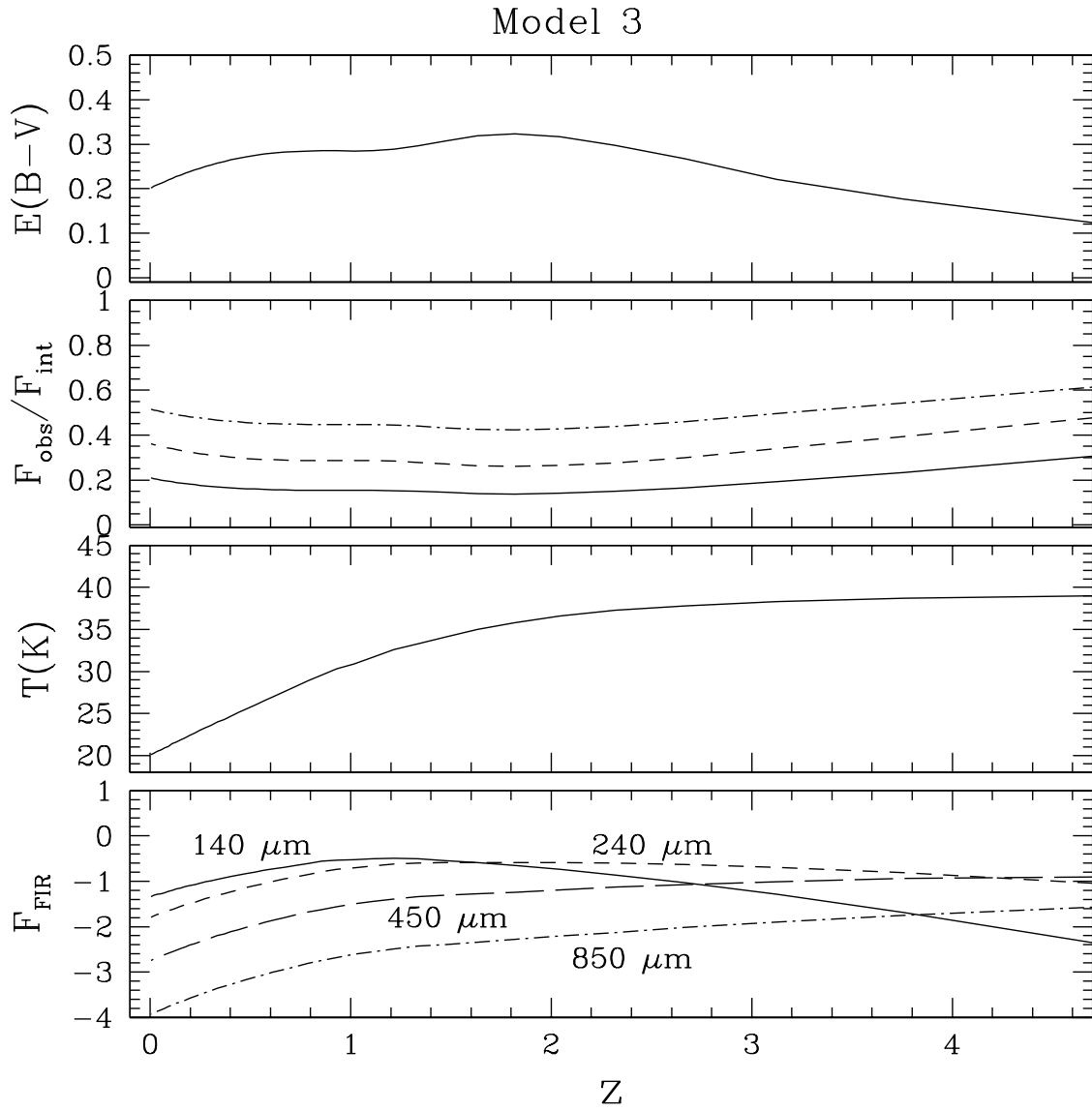


Fig. 9.— As Figure 6, for  $\text{SFR}_{\text{int}}$  of Model 3.

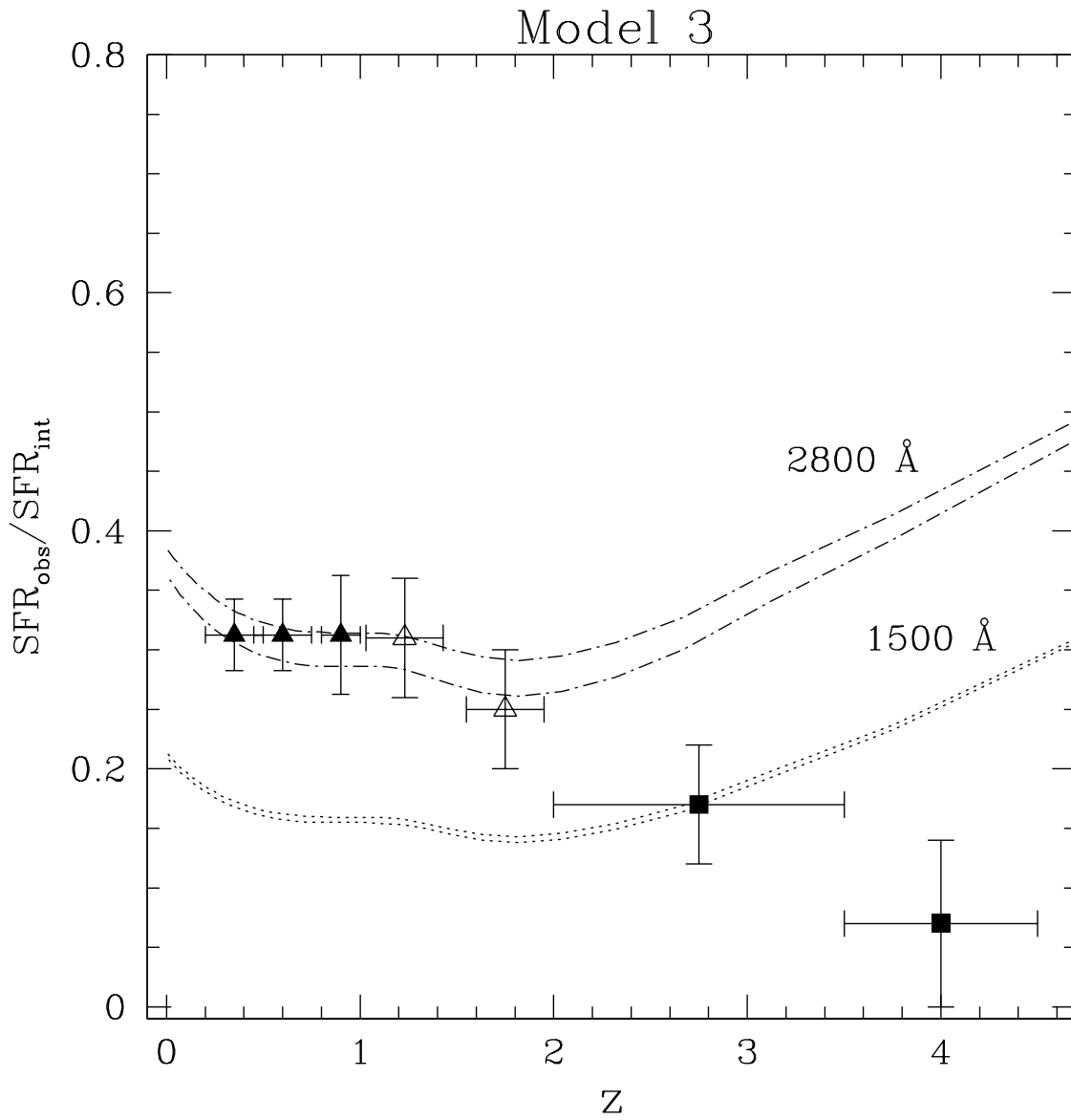


Fig. 10.— As Figure 4, for the  $\text{SFR}(z)$  of Model 3. The agreement between  $\text{SFR}_{\text{int}}/\text{SFR}_{\text{obs}}$  and predicted UV opacities implies that  $\text{SFR}_{\text{int}}$  of Model 3, as Model 2, is also a solution of our self-consistent procedure.

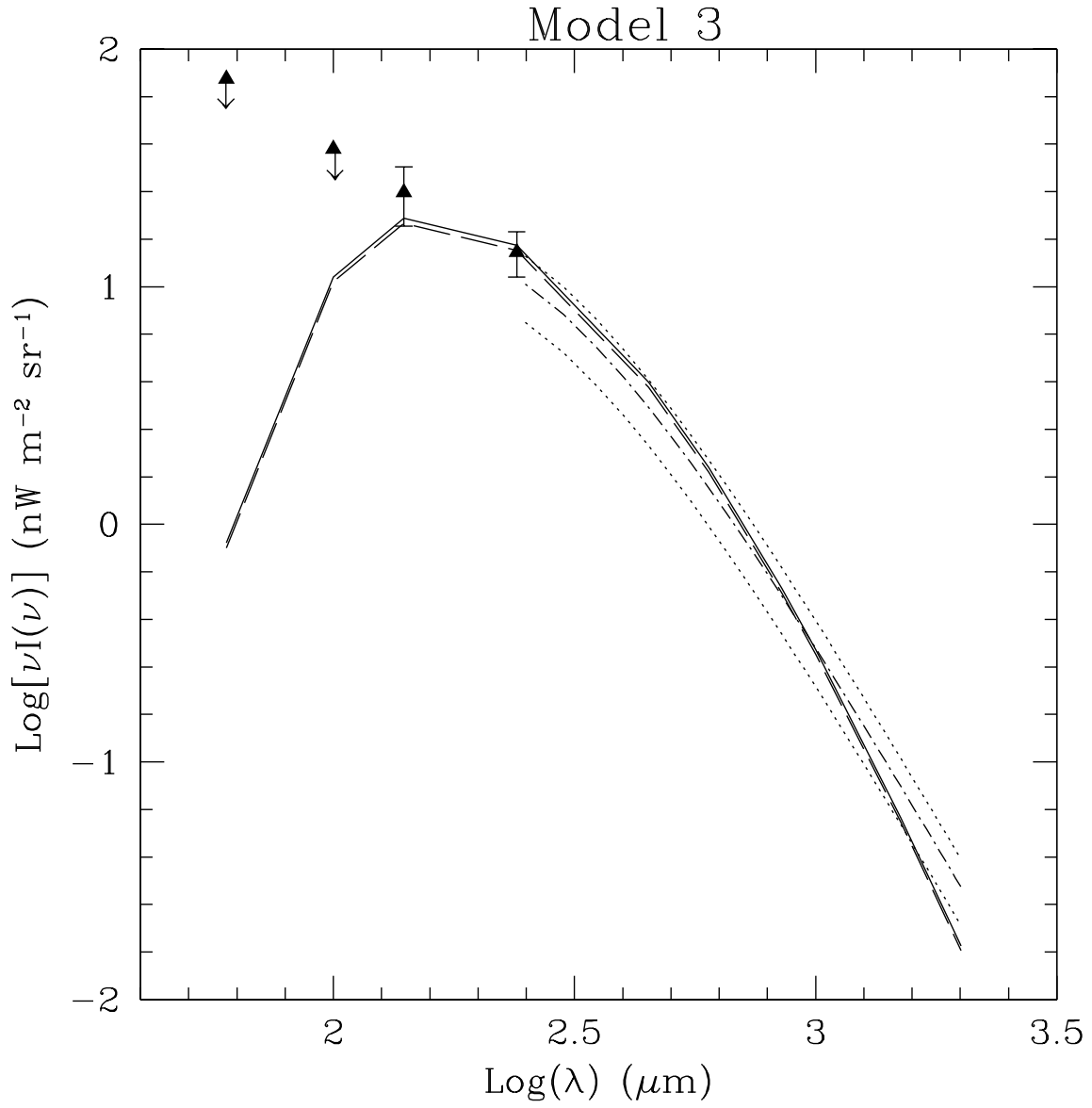


Fig. 11.— The FIR background predicted by the  $\text{SFR}_{int}$  of Model 3 is compared with the data from COBE DIRBE and FIRAS. The symbols and lines are as in Figure 5.

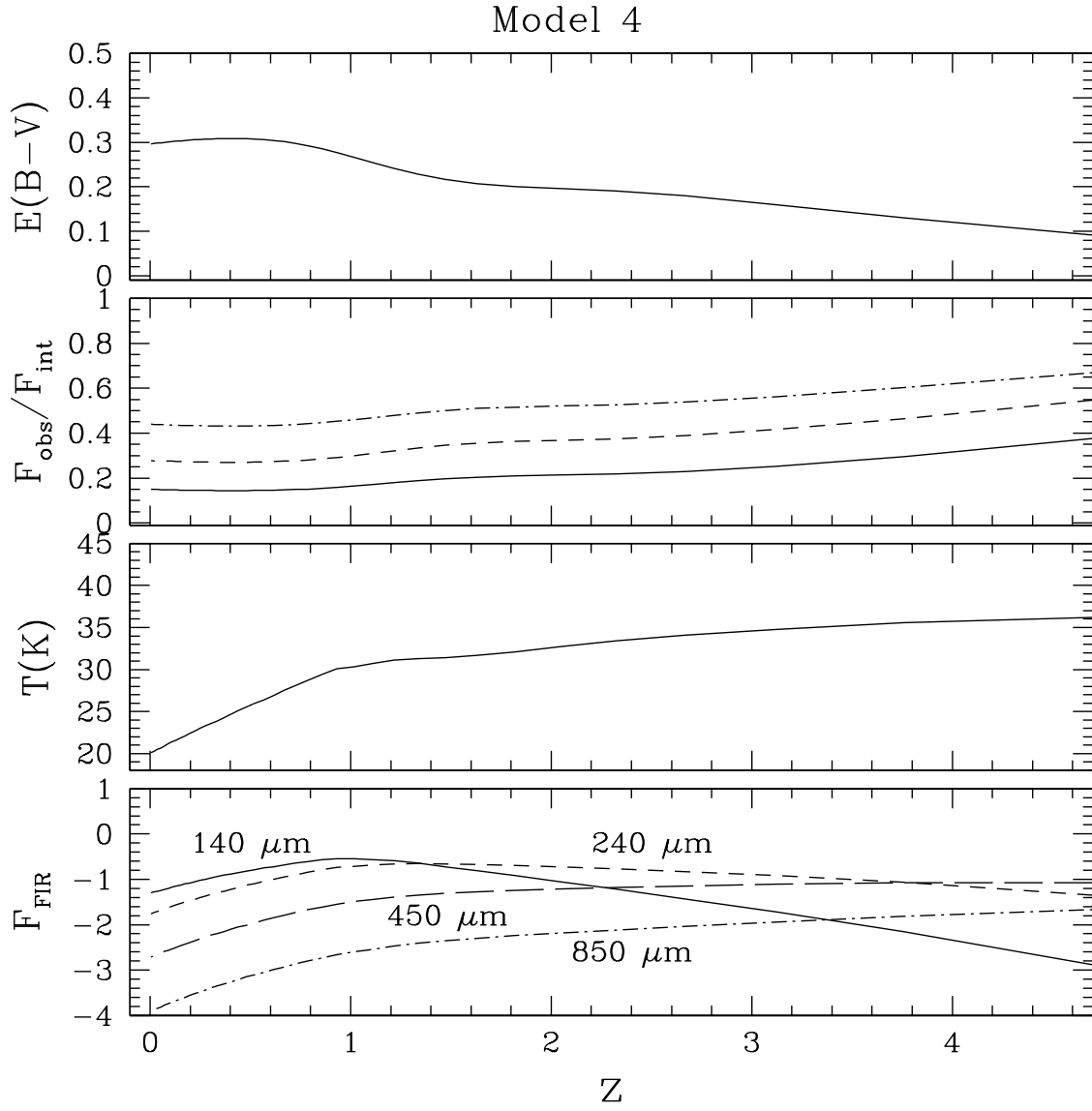


Fig. 12.— As Figure 6, now for  $\text{SFR}_{\text{int}}$  of Model 4.

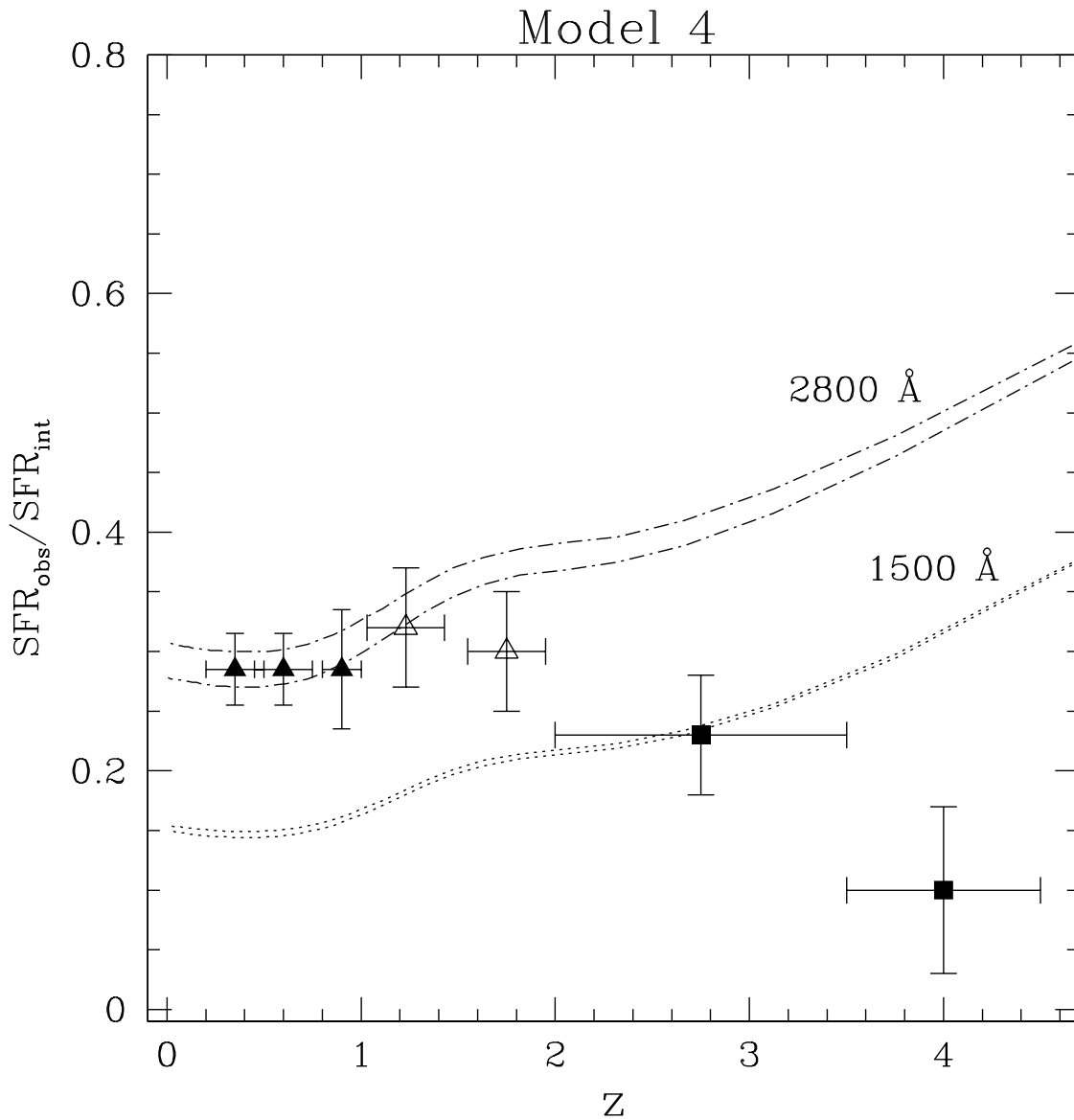


Fig. 13.— As Figure 4, for the  $\text{SFR}(z)$  of Model 4. The agreement between  $\text{SFR}_{\text{int}}/\text{SFR}_{\text{obs}}$  and predicted UV opacities implies that  $\text{SFR}_{\text{int}}$  of Model 4 is another acceptable solution of the self-consistent procedure.

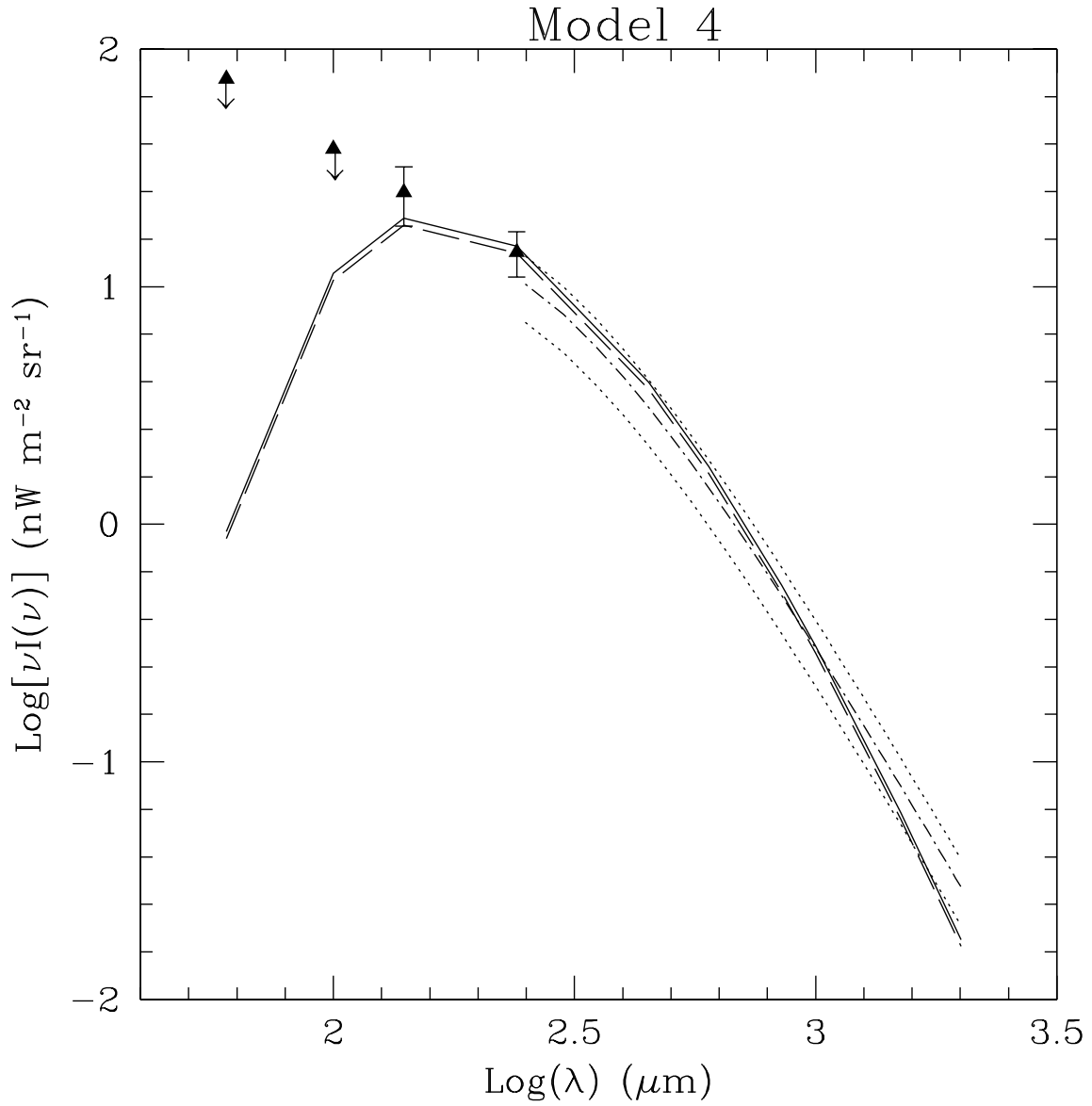


Fig. 14.— The FIR background predicted by Model 4 is compared with the data from COBE DIRBE and FIRAS. The symbols and lines are as in Figure 5.

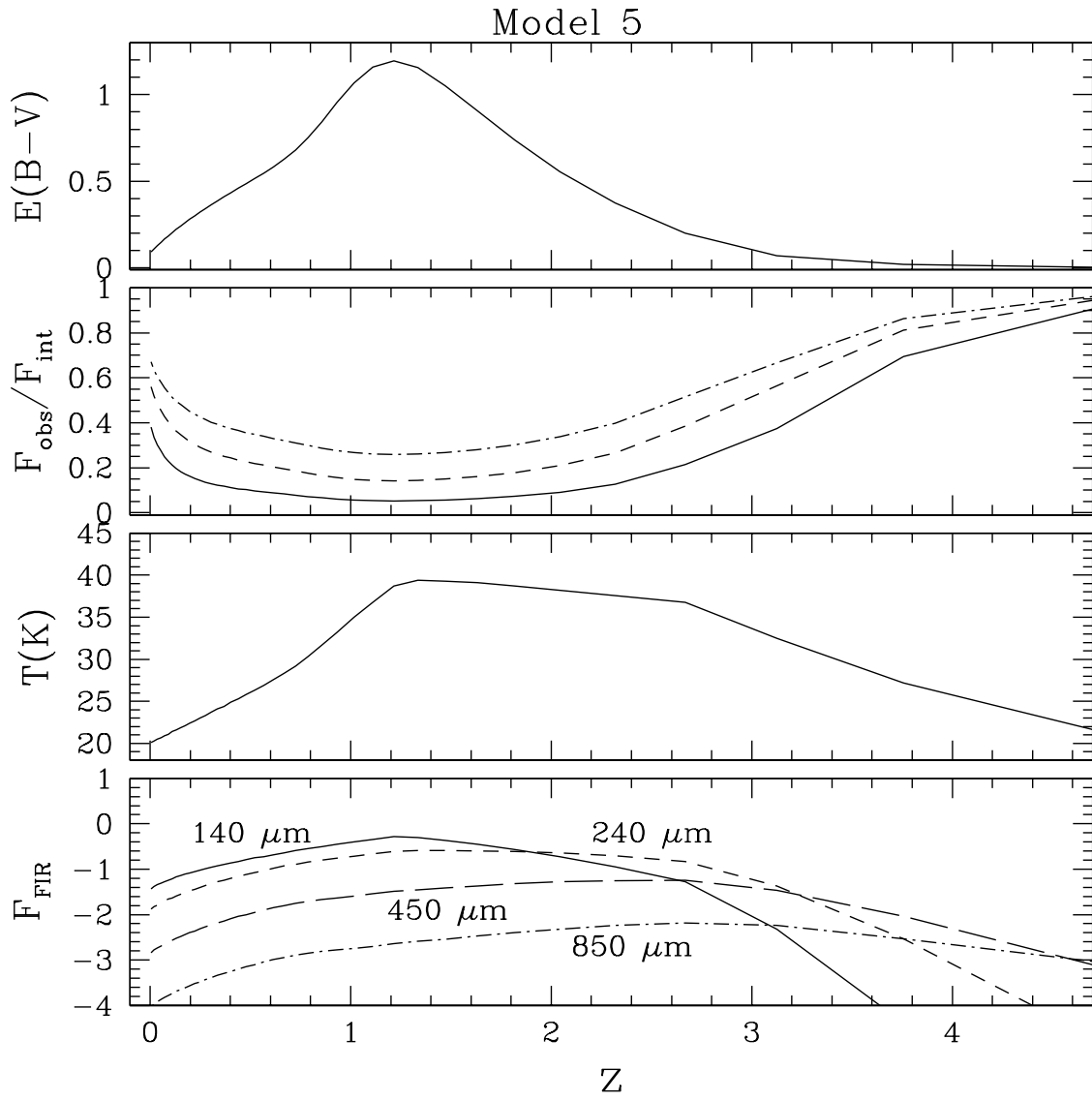


Fig. 15.— As Figure 6, for  $\text{SFR}_{\text{int}}$  of Model 5.

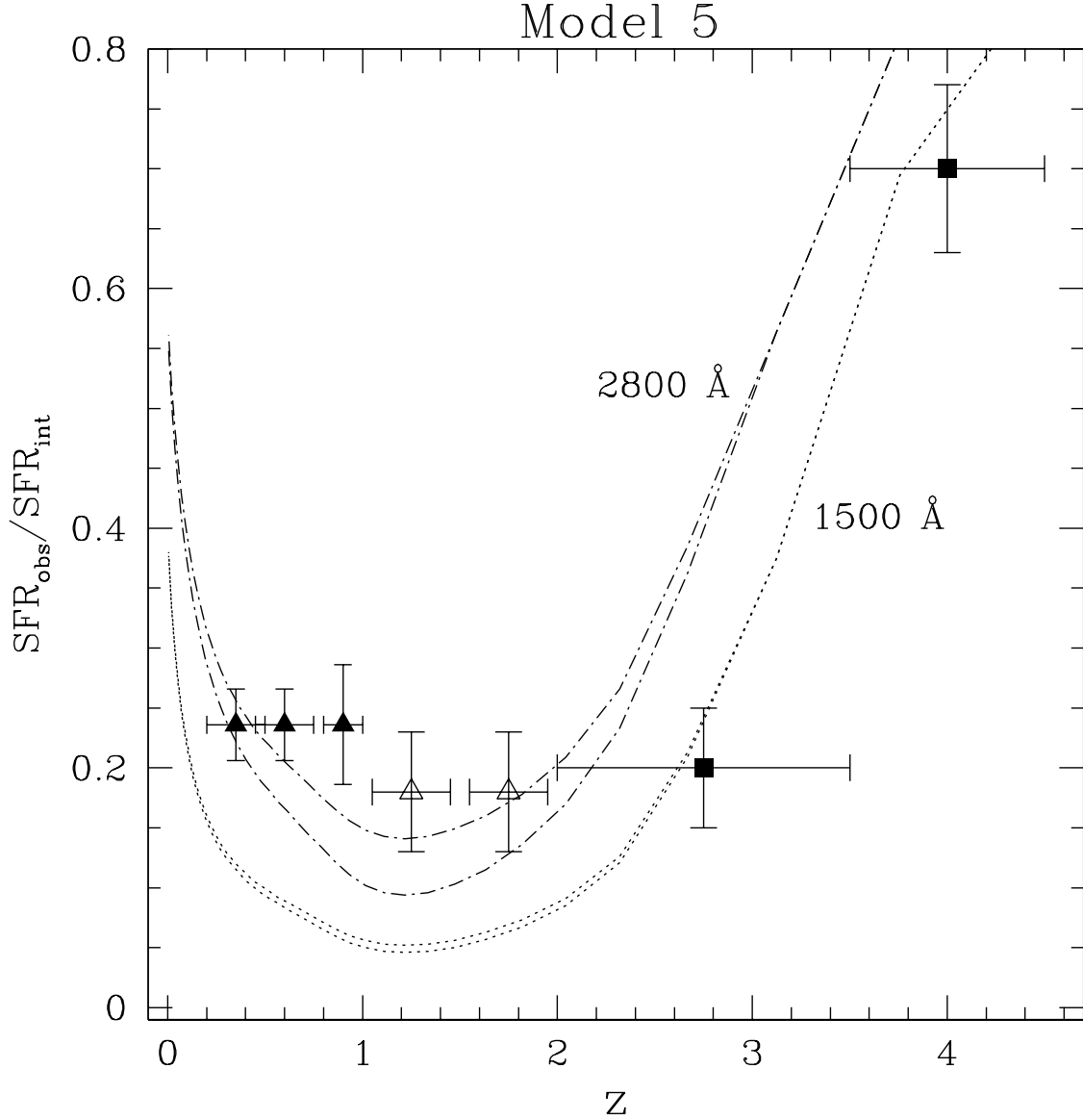


Fig. 16.— As Figure 4, for the  $\text{SFR}(z)$  of Model 5. The  $\text{SFR}_{\text{obs}}/\text{SFR}_{\text{int}}$  points at  $z=2.75$  and at  $z=4$ , which are equivalent to the emergent-to-total light at  $1500 \text{ \AA}$ , overlap with the predicted opacity curve at the same wavelength. The  $\text{SFR}_{\text{obs}}/\text{SFR}_{\text{int}}$  at  $z < 2$ , however, does not reproduce the curve of the emergent-to-total light at  $2800 \text{ \AA}$  as well as the previous three models do. This figure shows that the  $\text{SFR}_{\text{int}}$  of Model 5 is almost a solution for the iterative procedure, but the  $\text{SFR}_{\text{int}}/\text{SFR}_{\text{obs}}$  does not completely account for the predicted UV opacities.



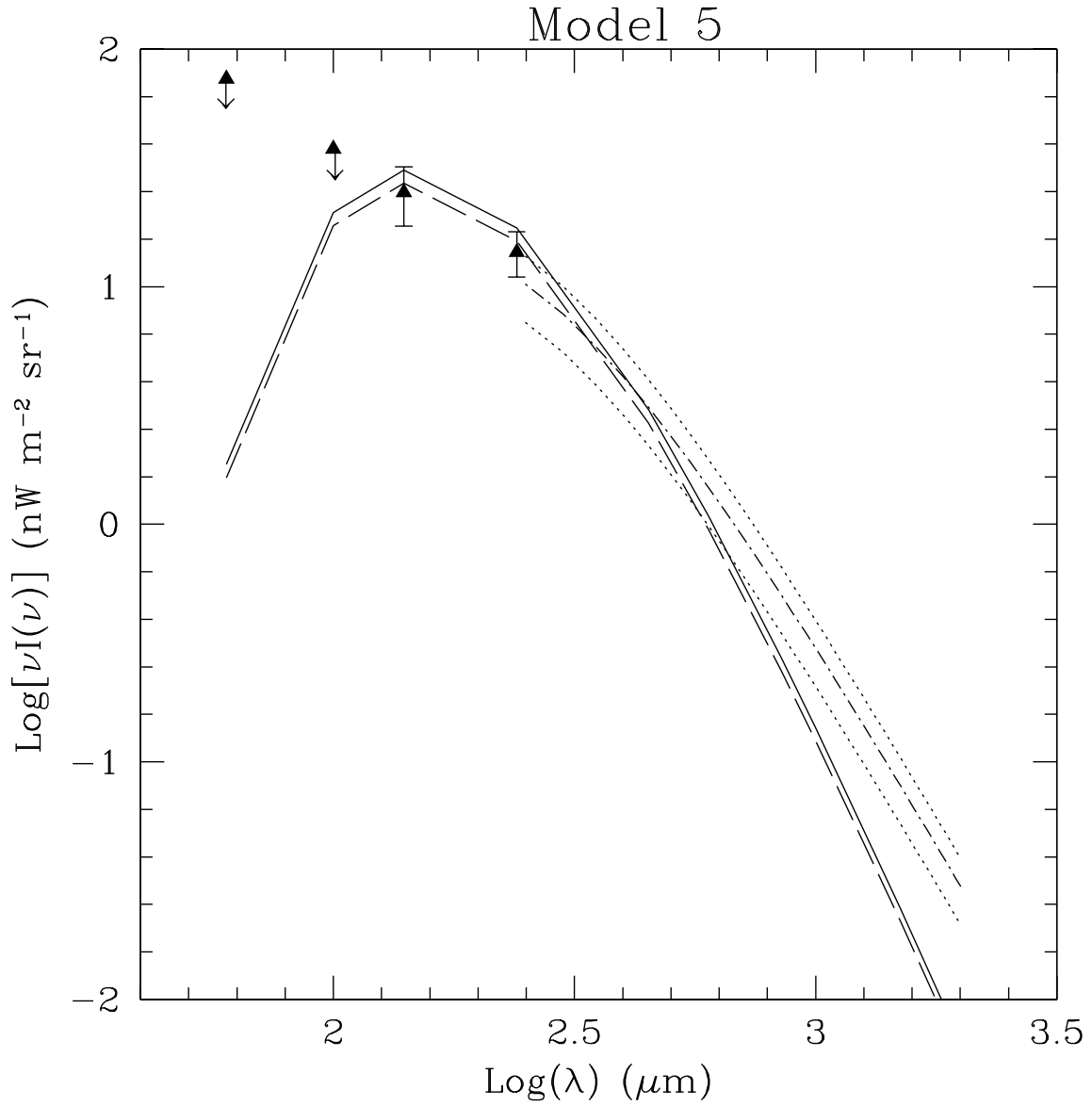


Fig. 17.— The FIR background predicted by the  $\text{SRF}_{int}$  of Model 5 is compared with the data from COBE DIRBE and FIRAS. The symbols and lines are as in Figure 5.

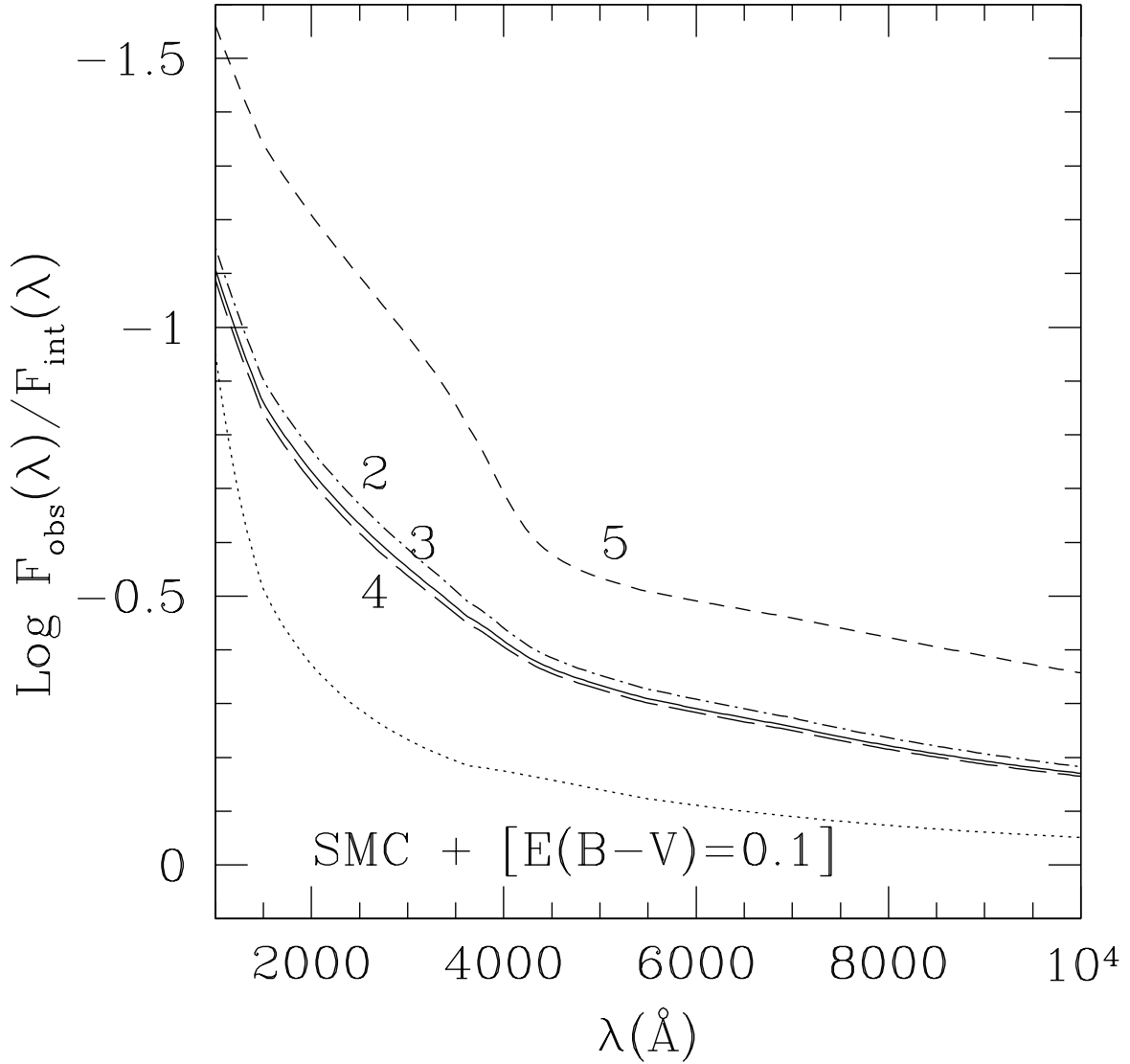


Fig. 18.— The relative and absolute attenuations predicted by Models 2 to 5 in correspondence of their *peak dust column densities*  $E(B-V)$  are plotted as a function of wavelength. Symbols and line conventions are as in Figure 3. For comparison, the attenuation produced by a foreground screen of dust with  $E(B-V)=0.1$  and an SMC curve is also shown. Models 2 to 4 produce relative attenuations which are comparable to the dust screen, but absolute attenuations about 50% higher. All Models are shown for the dust/star scaleheight ratio  $hh_1$ .

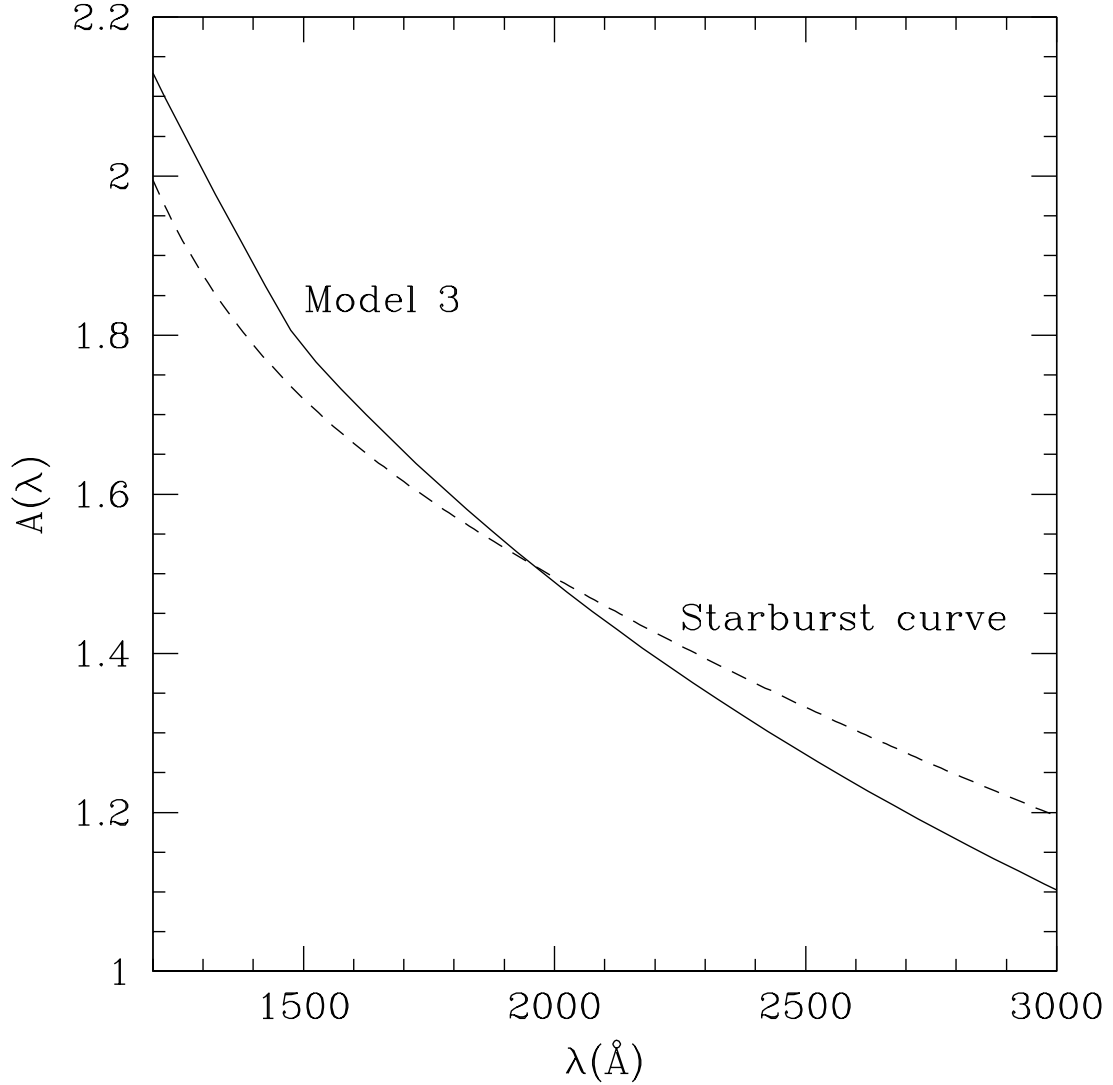


Fig. 19.— The attenuation  $A(\lambda)$  of a galaxy at  $z=3$  is shown as a function of wavelength in the UV range for Model 3 (solid line) and the ratio  $h_{dust}/h_{star}$  of  $hh1$ . For comparison, the attenuation produced by the ‘starburst’ reddening curve (Calzetti et al. 1994, Calzetti 1997), rescaled to match the attenuation from Model 3, is also shown (dashed line). The rescaling factor is  $E(B-V)=0.154$ . The two attenuations are similar, with the largest discrepancy being about 13% in the range 1200–3000 Å. Thus the starburst reddening curve can be used as an estimator of galaxy opacity at high redshift, provided the appropriate color excess  $E(B-V)$  is used.

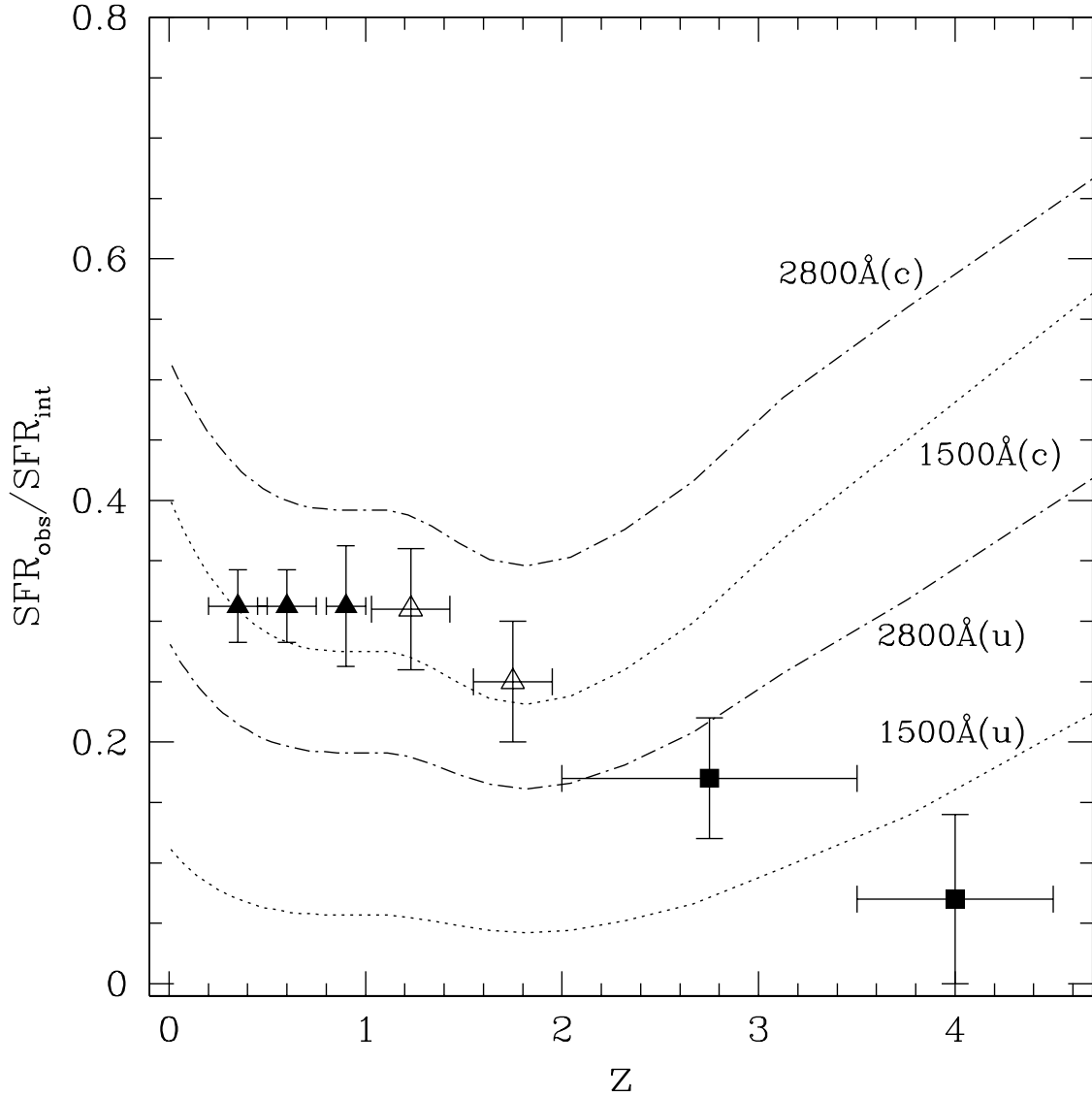


Fig. 20.— As Figure 10 (Model 3), for two different geometries of the dust/star distribution: (u) the dust distribution is a uniform shell surrounding the stars; (c) the dust distribution is a clumpy shell surrounding the stars. The emerging-to-total light ratios are shown at both 2800 Å (dash-dotted lines) and the 1500 Å (dotted lines). The ratio  $h_{dust}/h_{star}$  is given by hh1.

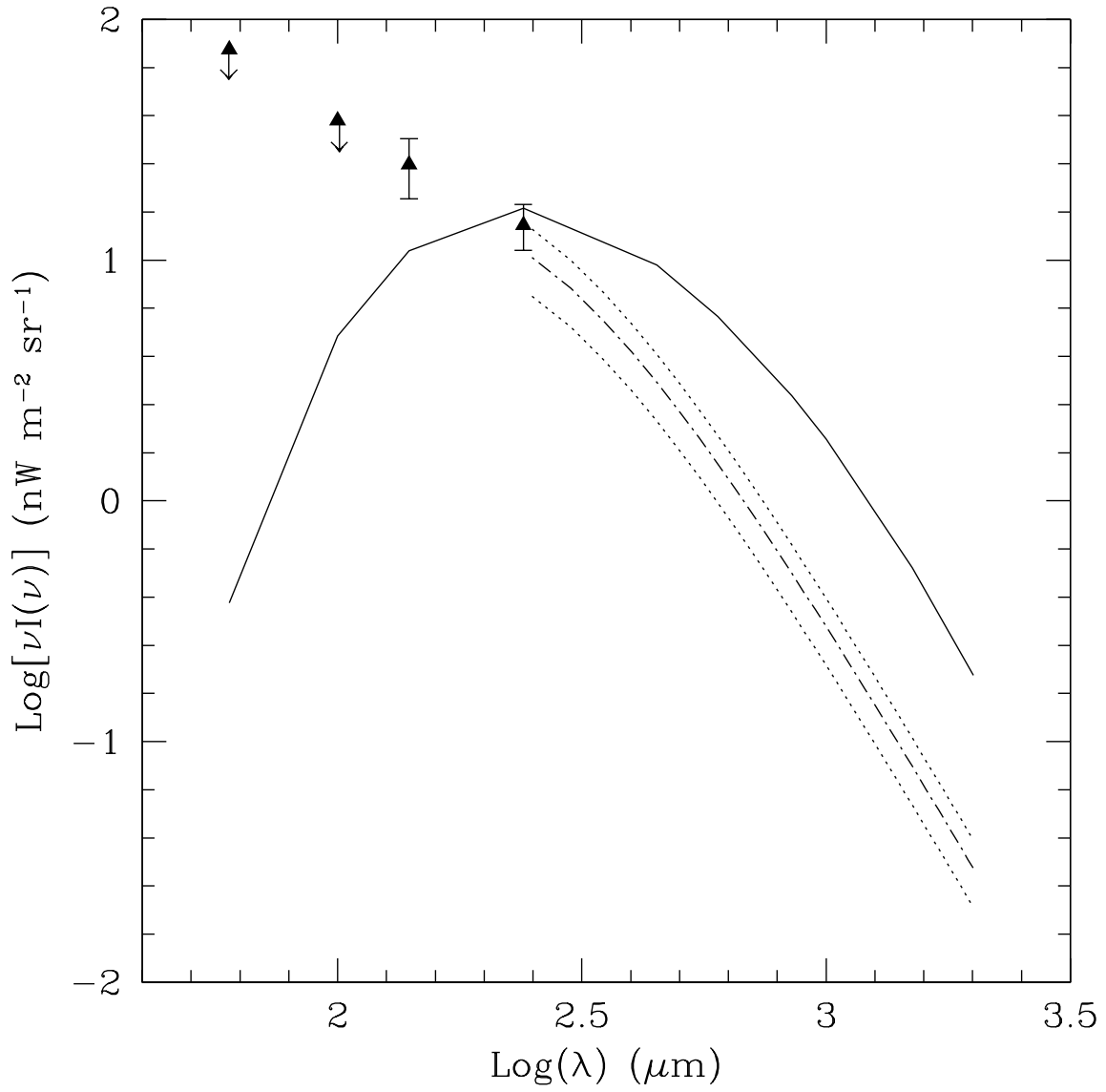


Fig. 21.— As Figure 11 (Model 3), for a constant temperature of the dust,  $T=21$  K.

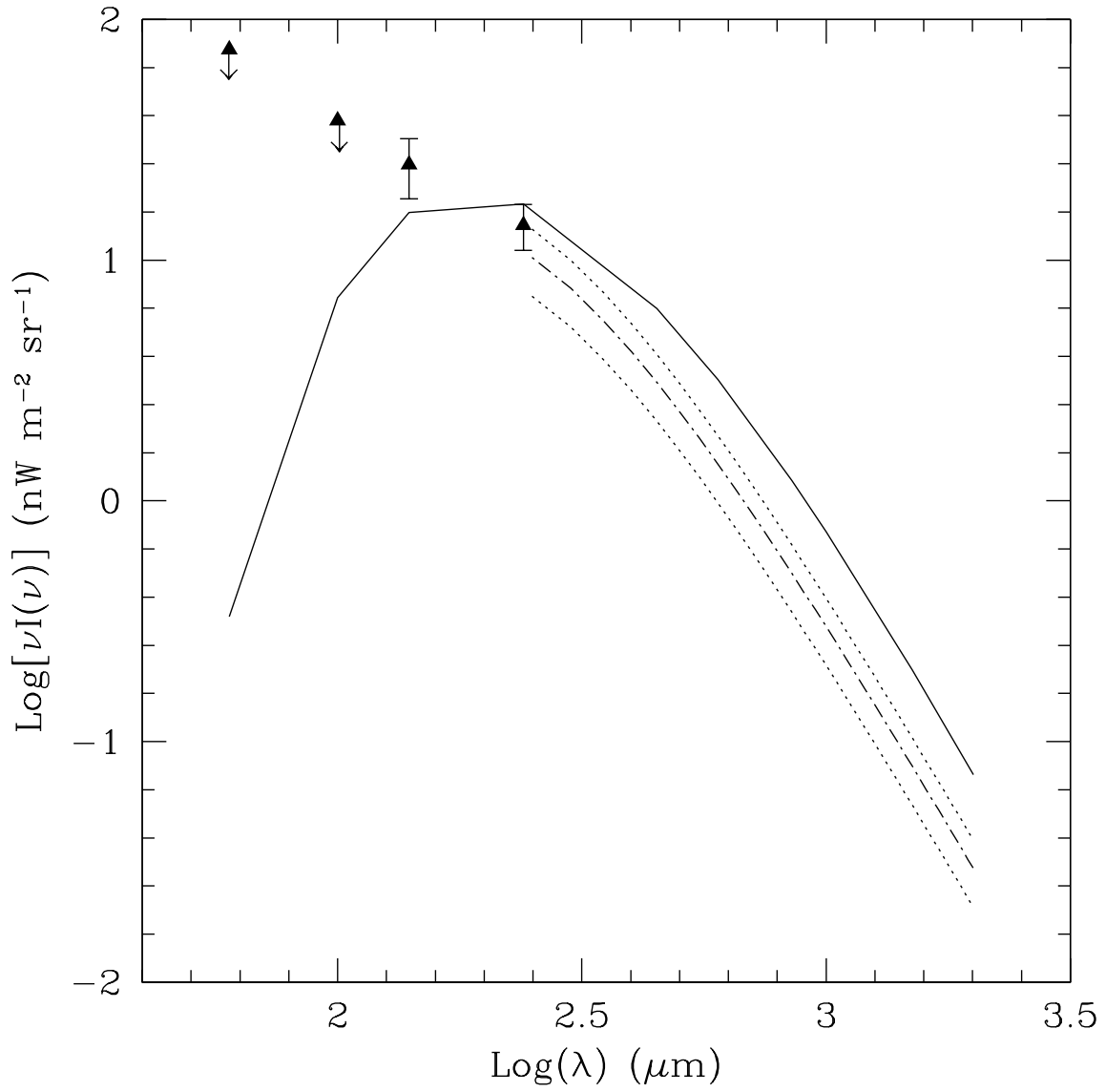


Fig. 22.— As Figure 11 (Model 3), for a dust emissivity index  $\epsilon=1$ .